OUKA
The University of Osaka
Institutional Knowledge Archive

Title	The Effect of Carbon on the Hydride Formation in Metals
Author(s)	原田, 修治
Citation	大阪大学, 1983, 博士論文
Version Type	VoR
URL	https://hdl.handle.net/11094/1820
rights	
Note	

The University of Osaka Institutional Knowledge Archive : OUKA

https://ir.library.osaka-u.ac.jp/

The University of Osaka

The Effect of Carbon on the Hydride Formation in Metals

Shûzi HARADA

March 1983

Department of Material Physics, Faculty of Engineering Science, Osaka University, Toyonaka, Osaka 560, Japan.

Abstract

Some metallic hydrides are promising materials as the safety container of hydrogen. Recently, it was observed that more amount of hydrogen was absorbed in carburized fcc Fe-Ni alloys and their hydrides were more stable than in carbon-free ones. The interstitial carbon atom will give strong electronic disturbances and lattice displacements on the surrounding metal atoms, and, therefore, will strongly influence the condition of hydride formation. In the present study, to investigate the behaviour of hydrogen in metals and to clarify the effect of carbon on hydride formation, the local electronic structures around an interstitial hydrogen and carbon atom were studied by means of ^{57}Fe Mössbauer effect in fcc Fe-Ni-H, Fe-Ni-C and Fe-Ni-C-H alloys. At the same time, to find the binding energy between metal and hydrogen atoms, the heat of dissociation of hydride in nickel and fcc Fe-Ni alloys with and without carbon was observed by means of thermal analysis. In parallel, that of Pd-H and Pd-C-H alloys was also investigated. Palladium belongs to the same periodic group as nickel, but the electronic structures are spacewise and energywise different from those of nickel. Based on the above experimental results, the nature of metal-to-hydrogen interaction in the above metals and alloys was discussed on the basis of the electron theory and lattice distortion theory and optimum conditions for hydride formation was suggested.

The Effect of Carbon on Hydride Formation in Metals

Contents

Chapter 1. Introduction

§1. General Introduction

Much attention has been paid to the problem of hydrogen in metals, because hydrogen atoms can be easily solved in most of metals[1] and bring about valuable or harmful properties in them. One of the useful applications is a safety container of hydrogen by appling the nature of hydride formation in metals[2-4] and another one is the purification of hydrogen by using high diffusivity of hydrogen in metals.[5] While, hydrogen embrittlement of steels is the most detrimental phenomena.[6,7] To investigate the above properties of metal-hydrogen systems, many studies have been carried out on the solubility,[8] interstitial position[9] and diffusion[5,10] of hydrogen in metals, electronic structures of metal-hydrogen systems,[2,11-13] lattice strains due to hydrogen atoms,[14] heat of reaction of hydrogenation[1,8,13] and so on.

Recently, Sohmura and Fujita found that the amount of absorbed hydrogen in the fcc $Fe_{69}Ni_{28}C$ alloy was larger and its hydride was more stable than in carbon-free one.[15] The interstitial carbon atoms are known to give strong electronic disturbances and lattice displacement on the surrounding metallic atoms,[16,17] and, therefore, will control the condition of hydride formation. This means that there is a possibility to clarify the suitable conditions for hydride formation by comparing the hydrogenated carbon-free and carburized alloy. In the present study, the local electronic structure of metal

atoms affected by carbon and hydrogen atoms will be investigated by means of the Mössbauer effect. At the same time, the bonding energy of metal-to-hydrogen atoms in the carburized and carbon-free fcc Fe-Ni alloys will be measured by using a technique of thermal analysis. From the above experimental results, the mechanism of hydride formation will be discussed on the basis of the electron theory and the lattice distortion theory and the explanation of the effect of carbon on hydrogen absorption in fcc Fe-Ni alloys will be attempted in an extension of the above theories. In parallel, the effect of carbon on Pd-H alloy was also investigated, since the d-orbital configurations of palladium are spacewise and energywise different from those of nickel.[18)]

In the following six sections, a brief review of the behaviour of hydrogen and carbon in metals is given to help the understanding of the present study.

In chapter 2, the amount of absorbed hydrogen in palladium, nickel and fcc Fe-Ni alloys with and without carbon is introduced by means of hydrogen gas volumetric method. At the same time, the comparison of X-ray diffraction profiles in the each corresponding alloys is shown.[19)]

In chapter 3, the Mössbauer effect study of fcc Fe-Ni-C and fcc Fe-Ni-H alloys is given. By this method, the environmental effect of interstitial elements on the matrix atoms is precisely studied, and the change of the local electronic structure around an interstitial atom is interpreted on the basis of the electron theory.[20)]

In chapter 4, it is shown that thermal analysis on hydrogen outgassing process of Pd-H, Ni-H and fcc Fe-Ni-H alloys is done and the bonding energy of between metal and hydrogen atoms is obtained. In addition, the theoretical evaluation of the energy of outgassing process is given in terms of the elastic dipole interaction and electronic metal-hydrogen interaction, and the mechanism of hydride formation is described.[21]

In chapter 5, thermal analysis and Mössbauer spectroscopy of carburized Pd-H, Ni-H and fcc Fe-Ni-H alloys are introduced and the effect of carbon on the stability of hydrogen in metals is shown on the basis of the lattice distortion theory and electron theory.[22]

§2. Types of Hydrides and their Applications[1,13]

The term "hydride" is defined as a compound having a metal-to-hydrogen bond. According to the bonding nature, the metal-hydrogen systems are generally classified into three categories as covalent, ionic and metallic. However, the distinction between the three types does not always exist. For instance, some metallic hydrides such as Ni-H and Cu-H exhibit both metallic and covalent character.

Typical covalent hydrides are of aluminium and silicon which belong to groups IB to IV B. In general, valence electrons are shared on a fairly equal basis between the elements. These hydrides for the most part are extremely poisonous and burn easily in air. Their applicability is

very little. Ionic hydrides, for instance Na-H and Li-H belonging to groups IA and II A, are bounded by strong electronegativity. These hydrides exhibit large heats of formation and high melting points, and are utilized as a reducing agent of chemical reaction. Metallic hydrides are formed by the transition metals and hydrogen atoms such as the specimens used in this study and have useful applications as a hydrogen storage material which is free from danger of explosions. In general, the packing density of hydrogen in metallic hydride is considerably higher than that of solid hydrogen at 14K, and, some hydrides are stable at room temperature.

§3. Interstitial Positions of Hydrogen and Carbon and Induced Lattice Strains[9,14,23)]

By means of neutron diffraction, it was found that hydrogen atoms occupy the interstitial octahedral sites in the metals and alloys used in this work, which have the face centered cubic structure. When hydrogen atoms are absorbed into a metal, an increase of lattice parameter is observed, and, in general the unit cell volume of the host lattice increases in proportion to the hydrogen concentration. The unit cell volume increment per hydrogen-metal ratio is 0.29 $\mathring{A}^3$/(0.1H/M) for palladium and nickel.

The carbon atoms also occupy the octahedral sites of the fcc lattice. The volume change of the unit cell per unit carbon concentration for the above metals is 0.67$\mathring{A}^3$/(0.015C/M),

which is considerably larger than that of hydrogen.

§4. Diffusion of Hydrogen[5,10]

The diffusion coefficient, D, of hydrogen in metals is extremely larger than that of other interstitial atoms such as carbon and nitrogen. The D value of hydrogen and carbon in nickel is $2.49\times10^{-9}cm^2/s$ and $1.04\times10^{-26}cm^2/s$ at room temperature, respectively,[24] and, therefore, the mean migration distance, $(2Dt)^{1/2}$, is evaluated to be $7\times10^{-5}cm$ for hydrogen, while that of carbon is $1.4\times10^{-13}cm$ at room temperature. The migration energy of hydrogen in nickel is 36 kJ/mol in the range of 653-1273K. Recently, in the low temperature range below 300K, the tunneling effect of hydrogen atoms in nickel has been found by Yamakawa[25] and Tada and Fujita.[26] The migration energy of carbon in nickel is 145 kJ/mol in the range of 1293-1673K.

§5. Electronic Structure of Metal-Hydrogen Systems

In order to clarify the electronic structures of transition metal-hydrogen alloys, several experimental techniques such as the Mössbauer effect,[27,28] photo emission spectroscopy,[29,30] nuclear magnetic resonance (NMR),[31] magnetic susceptibility[13] and electrical resistivity measurement[32] have been applied. Mössbauer spectroscopy of metal-hydrogen systems mostly using ^{57}Fe isotope have been carried out, for instance, on Fe-Ni-H,[33-35] Fe-Pd-H,[36,37] Ni-H,[38,39] Nb-H[40] and Ti-H[41], the latter three containing ^{57}Fe

probe isotope. In general, the internal magnetic field of iron probe atoms decreases with the increase of hydrogen concentration and the change of isomer shift of probe atom is positive by hydrogenation. This reduction of internal field and change of isomer shift have been interpreted in recent theoretical studies,[42,43] and will be also discussed in detail in chapter 3. According to the result of the molucular orbital calculation with the cluster model by Adachi and Imoto,[42,43] the bonding level between metal and hydrogen atoms is induced below the bottom of the d-band by s-d hybridization and electron transfer occurred between an interstitial atom and surrounding metal atoms, which gives rise to the increase of the Fermi level. Formation of the metal-hydrogen bonding level and the increase of the Fermi level can be detected by photo emission spectroscopy. For instance, Eastman et al.[28] have observed a band of hydrogen induced energy states centerd at leV below the bottom of Pd-derived d band of the width of 4.4eV. The electronic structure of hydrogen in metal is investigated by means of high resolution NMR spectrometer. From the negative values of Knight shift of hydrogen atoms in V-H alloys relative to a proton signal from water, a protonic model for hydrogen atoms in metal has been proposed by Kazama and Fukai,[44] where protons were surrounded by a cloud of screening electrons.

The fcc Fe-Ni alloys in the concentration region around 35 at.% nickel are called Invar alloys, which have their

peculiar properties such as small thermal expansion coefficient, large magneto striction, small Young's modulus, etc.[45,46] Usually, the magnetic properties of Invar alloys are fairly complex, Fe-Ni Invar alloys are located in a magnetic region such as a drastic decrease of the saturation moment from the top of the Slater-Pauling curve in the iron rich side. Mössbauer spectroscopy on the Fe-Ni Invar alloys shows that a part of the iron atoms is situated on weak ferromagnetic states in addition to the normal strong ferromagnetic ones.[47-49] Sohmura and Fujita[15,36,37] showed that the characteristic weak ferromagnetic components in the Mössbauer spectra disappeared by hydrogenation, and, at the same time, pointed out the disappearance of the characteristic small thermal expansion. In this paper, the detail Mössbauer effect of hydrogenated fcc Fe-Ni Invar and non-Invar alloys will be done, and the disappearance of weak ferromagnetic components by hydrogenation will be discussed on the basis of the electron theory.

§6. Electronic Structure of Metal-Carbon Systems

Mössbauer effect studies of bcc Fe-C,[16,50] Fe-Mn-C[17] and Fe-Ni-C[51] alloys all of which have the bcc structure have been done in detail by Fujita et al. They observed many sub-peaks due to interstitial carbon in the Mössbauer spectra. Precise spectral analyses have revealed that the iron atoms first-neighbouring with the interstitial carbon atoms have considerably smaller values of internal magnetic

field than those in carbon-free alloys, while the internal field of the second and third neighbour irons is slightly larger than that of carbon-free ones. A recent theoretical study by Adachi and Imoto[52] based on the DV-Xα cluster method in the molecular orbital calculation showed that the iron-carbon bonding level similar to metal-hydrogen bonding as mentioned in the last section was induced below the bottom of the d-band and electron transfer occurred between the carbon and surrounding iron atoms, giving rise to a remarkable reduction of the internal field of the first-neighbouring iron atoms. In this paper, the environmental effect of interstitial carbon atoms on the matrix atoms not for bcc but for fcc carburized Fe-Ni Invar and non-Invar alloys will be discussed in detail specially in relation to the Mössbauer effect.

§7. Thermodynamics of Metal-Hydrogen Systems[53,54]

The equilibrium condition between hydrogen in a gas state and in a solid solution phase is given by the equation,

$$\bar{G}_H \text{ (in gas)} = \bar{G}_H \text{ (in solution)}. \qquad (1.1)$$

The partial molar free energy, $\bar{G}_H$, of hydrogen in a fcc metal is written by

$$\bar{G}_H \text{ (in solution)} = RT \ln \frac{X_H}{1-(2+\delta)X_H} + I \ , \qquad (1.2)$$

where δ is $Z_{H-H}\varepsilon_{H-H}/kT$, I is the binding energy, $Z_{M-H}\varepsilon_{M-H}$, of hydrogen in a metal and x_H is molar fraction of hydrogen atom, and Z and ε mean the coordination number and the bond energy, respectively. The partition function of hydrogen gas consisting of N molecules is given by $Q_B=q_H^N/N!$, where q_H is the partition function of a hydrogen molecule due to the translational, rotational and vibrational motions and written by

$$q_H = (2\pi mkT)^{3/2}(V/h^3)(T/2\theta_r)\{1-\exp(-\frac{\theta_v}{T})\}^{-1},$$

$2\theta_r$ and θ_v are 171K and 6140K for H_2, respectively,[50] where m, v and h are the mass of hydrogen, volume of system and Planck constant, respectively. By using the partition function, the partial molar free energy of hydrogen atom in a gas state is obtained by the following equation,

$$\bar{G}_H \text{ (in gas)} = \frac{1}{2}(-kT\frac{d}{dN}\ell n Q_B + E_D) = -kT\ell n\frac{q_B}{N} + E_D/2, \quad (1.3)$$

where E_D is the dissociation energy of hydrogen molecule. The solubility of hydrogen in metals is controlled by the equilibrium condition, eq. (1.1).

The dissolution process of hydrogen into metals is classified into exothermic and endothermic process by using the heat of solution, $I-E_D/2$ in eqs. (1.2) and (1.3). Typical exothermic metals with hydrogen, i.e. $I-E_D/2<0$, are, for instance, Ti, V, Nb, Zr and Pd, which form hydrides. While, Cr, Fe, Co, Ni and fcc Fe-Ni alloys belong to endo-

thermic metals, in general, and do not compose hydride except for nickel and fcc Fe-Ni alloys.[1,8,13)]

Chapter 2. The Effect of Carbon on the Amount of Hydrogen Absorption in Pd, Ni and fcc Fe-Ni Alloys

§1. Introduction

As mentioned in the last chapter, it was found that fcc $Fe_{69}Ni_{28}C_3$ Invar alloy in which carbon was added in order to stabilize the fcc phase absorbed more amount of hydrogen than carbon-free one. On the other hand, in the bcc steel, the amount of hydrogen decreased with the increase of carbon concentration.[55] Carbon atoms give strong disturbances on the surrounding metallic atoms, changing the electronic states and producing the local lattice distortion in its vicinity, and, therefore, will control the condition of hydride formation.

This chapter shows that the effect of carbon on the amount and stability of hydrogen absorbed in palladium, nickel and fcc Fe-Ni alloys which have the same crystal structure is studied by means of hydrogen gas volumetric method, X-ray diffraction and the measurement of dissociation temperatures of hydrides. Palladium is classified into the VIII A group in the periodic table as well as nickel. However, palladium makes more stable hydride than nickel hydride, and the metal belongs to the paramagnetic materials, which differs from ferromagnetic nickel. These unlike manners may be produced by the difference of the d-orbital configuration between the two metals,[50] and, therefore, we may expect that carbon in palladium hydride behaves in a different

way than in nickel hydride in absorption.

§2. Experimental Procedures

The fcc Fe-33Ni at.%Ni Invar alloy (hereafter referred to as Fe-33Ni), Fe-35Ni Invar alloy and the fcc Fe-45Ni, Fe-64Ni and Fe-75Ni non-Invar alloy were made by melting electrolytic iron and 99.9 at% pure nickel in an induction furnace. The ingot was homogenized at 1100°C for 60 hours, and cold-rolled to a sheet with the thickness of about 90μm. A plate of 99 at.% pure palladium and nickel were also cold-rolled to the same thickness. A half-cut of each metal sheet was used as the carbon-free specimen, and the other half was carburized in the methane and hydrogen mixed gas at 900°C for 4 hours,[57] and then homogenized at 1100°C for 48 hours. The sheet was rolled to thin plates, annealed at 900°C for 1 hour, quenched into iced water, and polished electrolytically. The final dimensions of the foil specimens were 30μm in thickness and 1.00cm in radius.

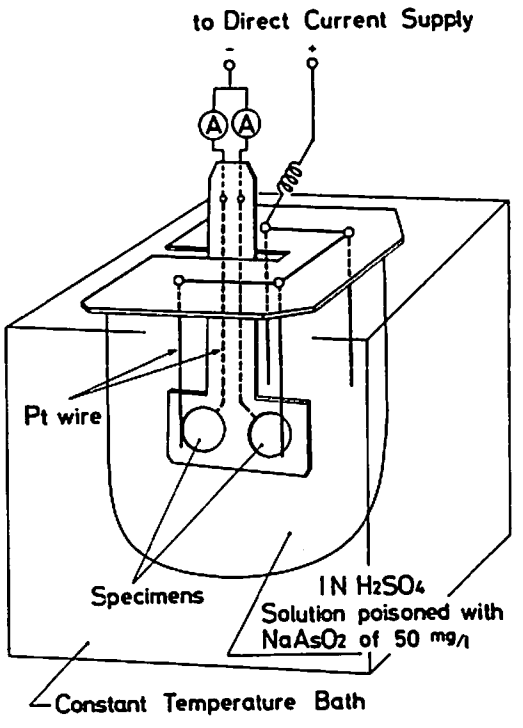

Fig. 1 Apparatus for cathodical hydrogen charging.

Hydrogen was supplied electrolytically in the 1N-H_2SO_4 solution poisoned with $NaAsO_2$ of 50mg/ℓ[58] with the current density of 0.16A/cm^2

at 20°C. The apparatus for hydrogen charging is schematically shown in Fig. 1. The charging time was 1000 mins.

Immediately after hydrogenation, X-ray diffraction measurement was carried out at 77K by using CoK radiation.

The amount of absorbed hydrogen was measured by collecting the released gas in a glycerine and triethyleneglycol mixture bath at 70°C for Ni-H and Fe-Ni-H alloys as shown in Fig. 2. The gas volumetric method in a vacuum cell in Fig. 3 was used for Pd-H alloy.

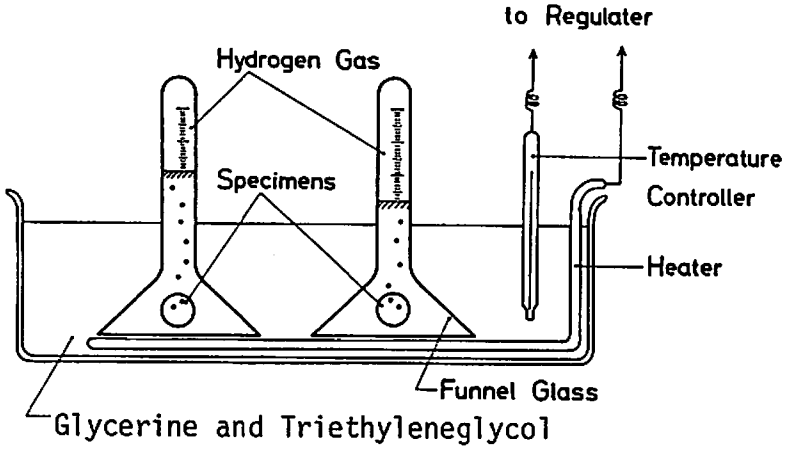

Fig. 2 Apparatus for hydrogen gas volumetiric method.

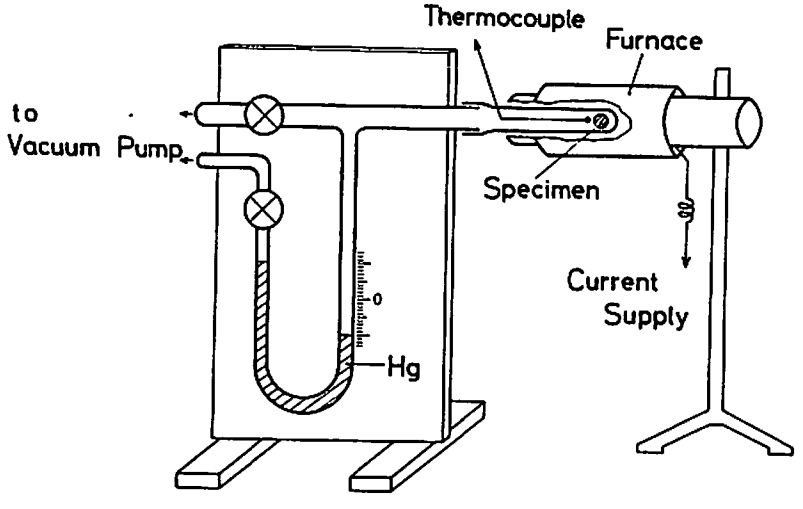

Fig. 3 Vessel used for hydrogen gas volumetric method

The concentration of carbon was controlled to be 1.5 at.% in all carburized alloys and checked by X-ray measurements of the lattice constant.[23,59] Precipitations such as cementite and graphite were not obserbed on the X-ray profiles and Mössbauer data. The phase diagrams of Pd-C and Ni-C system are shown by Hansen and Anderko[60] and that of Fe-Ni-C system is given by Kase.[61]

§3. Results and discussion

3.1 Amount of absorbed hydrogen

Figure 4 shows the amount of absorbed hydrogen in fcc Fe-Ni alloys and pure nickel with and without carbon against the nickel concentration. All these carburized fcc Fe-Ni alloys dissolve more amount of hydrogen than the corresponding carbon-free ones. The particular difference of the effect of carbon on hydrogen absorption between Invar and non-Invar alloys was not recognized. On the other hand, the carburized palladium absorb less amount of hydrogen than that in pure palladium, as shown along the right hand side coordinate of the

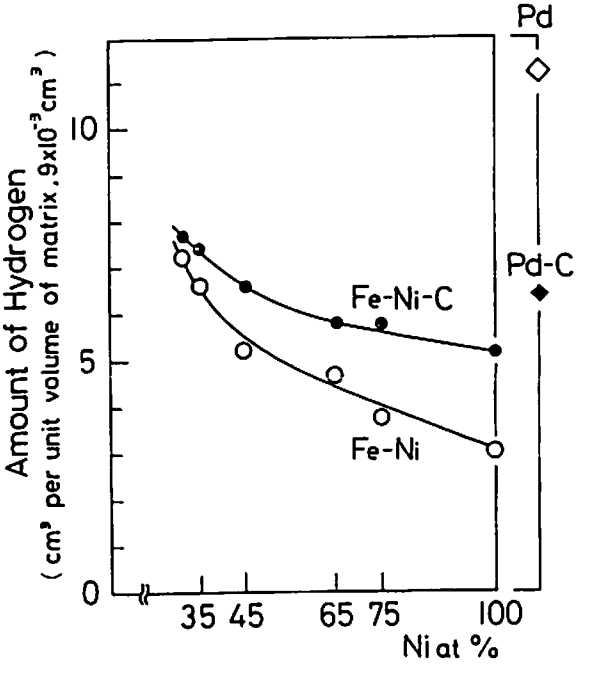

Fig. 4 Amount of absorbed hydrogen in fcc Fe-Ni and Fe-Ni-C alloys, nickel and Ni-C alloy and palladium and Pd-C alloy.

figure.

To make sure of the above difference between palladium and Fe-Ni alloys in the effect of carbon on hydrogen absorption, the dependence of the amount of absorbed hydrogen on the carbon concentration, on the charging time of hydrogen[58] and on the thickness of specimens[62] were examined, and the consistent data with respect to the above result were obtained. For instance, the change of the amount of absorbed hydrogen was in proportion to the carbon concentration, and it smoothly increased with the charging times until a saturation was reached at around 1000 mins. In the range of the foil thickness from 10 to 40 μm of the specimens, the metal-hydrogen atomic ratio was approximately the same under the present charging conditions.

3.2 X-ray diffraction profiles of hydrogenated alloys.

Figures 5(a) and (b) show the X-ray diffraction profiles of hydrogenated fcc Fe-33Ni and Fe-33Ni-C alloy. Two peaks in both profiles correspond to the hydride β_2 and β_1 phases which have a fcc lattice, and the broken lines in the figures mean the X-ray (200) diffraction peaks of hydrogen-free alloys. From the relative change of the peak positions from the broken lines in the figures, lattice expansion of β phase in carburized Fe-33Ni alloy was found to be slightly larger than that in carbon-free one. While, as shown in Figs. 5(c) and (d), lattice expansion of β phase in carburized nickel was slightly less than that of carbon-free one in spite of

the increase of the total amount of absorbed hydrogen which is shown in Fig. 4, where α means the hydrogen solid solution phase. Since the increase of the unit cell volume of fcc lattice is in proportion to the hydrogen concentration,[14,23] the above results suggest that the enhancement of hydrogen absorption in Fe-33Ni-C alloy is due to the increase of hydrogen concentration in β phase, while that in Ni-C alloy is due to the increase of regions of hydride phase as was

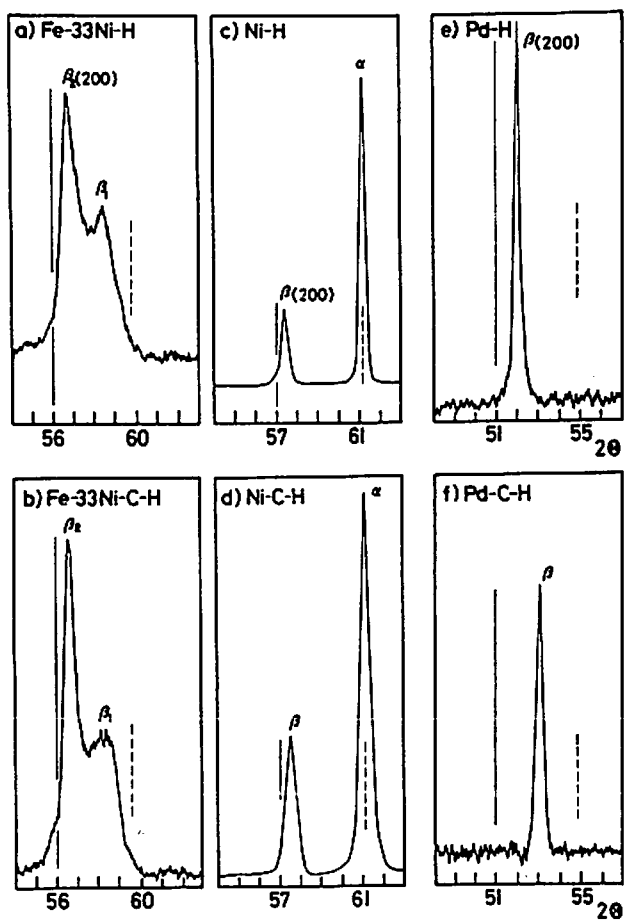

Fig. 5 X-ray (200) diffraction profiles of hydrogenated alloys at 77K.
a) Fe-33Ni-H. c) Ni-H. e) Pd-H.
b) Fe-33Ni-C-H. d) Ni-C-H. f) Pd-C-H.
The broken line in the figure is the X-ray (200) diffraction peak of hydrogen free alloys. The solid line is a reference line.

recognized from the increase of the peak intensity ratio, β/α, of X-ray profile. Figures 5(a) and (f) show the profiles of hydrogenated palladium and Pd-C alloy, and in this case, only the single phase was observed. Lattice expansion of β phase in Pd-C alloy was far less than that of palladium, and, therefore, the hydrogen concentration in Pd-C-H hydride must be considerably lower than in carbon free one.

3.3 Stability of hydrides

The stability of hydrides can be estimated from the dissociation temperature and the time of outgassing process. A dissociation time becomes longer with increasing nickel concentration in fcc Fe-Ni alloys at room temperature. While, the dissociation of Pd-H alloys can be performed at temperatures as high as 300°C. In other words, the stability of hydrides becomes low in order of palladium, nickel and fcc Fe-Ni alloys.

When Fe-33Ni alloy was carburized, the dissociation time became longer, while the dissociation temperature of Pd-C-H alloy was lower than that of carbon-free one. That is, the hydride became more stable when Fe-33Ni alloy was carburized, while the hydride in palladium became less stable by carburization. The quantitative measurements of the stability of the hydrides by means of thermal analysis will be introduced in chapters 4 and 5.

The above experimental results of the X-ray diffraction and the stability of hydrides revealed that the enhancement

or suppression of hydrogen absorption by carburization did not arise from a simple effect such as the lattice distortion by interstitial carbon atoms. The role of carbon on hydrogen absorption will be discussed on the basis of the electron theory and lattice distortion theory in chapter 5. In the next chapter, the local electronic structure around carbon and hydrogen atoms investigated by Mössbauer spectroscopy will be introduced and discussed.

Chapter 3. Mössbauer Effect of fcc Fe-Ni-C and fcc Fe-Ni-H Alloys

§1. Introduction

In this chapter, carburized fcc Fe-Ni Invar and non-Invar alloys and hydrogenated ones are investigated by means of ^{57}Fe Mössbauer spectroscopy. From the change of the local electronic structure around an interstitial atom, the environmental effect of interstitial atoms on Invar and non-Invar alloys is precisely studied and is interpreted on the basis of the electron theory and the lattice distortion theory.

As was mentioned in chapter 1, the Invar anomalies of fcc Fe-Ni alloys appear in the concentration region around 35 at.% nickel in which a drastic fall from the Slater-Pauling curve occurs and the peculiar properties such as small thermal expansion and large magnetostriction appear.[45,46] In the Invar region, the magnetic properties are complex, and several models have been proposed in order to interpret the above anomalies. In 1963, Weiss[63] proposed the two states model of fcc iron, in which iron atoms could take either the low spin state or the high spin state depending on the alloy concentration and temperature, and showed that Invar effect originated from the thermal excitation between two states. Recently, Kanamori and Teraoka[64] and Miwa[65] treated the problem with the extended CPA calculation which took account of the local environmental effect and pointed out various types of instability and fluctuation of the magnetic momemt

of iron atoms in the Invar region. On the other hand, Moriya and Usami[66] showed that the origin of the small thermal expansion of weakly ferromagnetic alloys, i.e., that of Invar alloys is a large negative thermal expansion due to the magneto-volume effect which is based on general spin fluctuations, and they also pointed out that the magneto-volume effect in ferromagnetic alloys produces the large positive thermal expansion. As an experimental method, Mössbauer spectroscopy is a powerful technique to investigate the magnetic structures on an atomic scale with respect to the Invar problem. Nakamura et al.,[47] Tomiyoshi et al.[48] and Gonser et al.[49] did the Mössbauer spectroscopy on the Fe-Ni Invar alloys and found independently that a large fraction of the iron atoms in the Invar alloys had weak ferromagnetic[47,48] or antiferromagnetic components[49] in addition to the normal strong ferromagnetic ones.

The fcc Fe-Ni alloys absorb large amounts of hydrogen and form fcc hydride as mentioned in the last chapter. Sohmura and Fujita showed that when the Fe-Ni Invar alloys are hydrogenated the characteristic weak ferromagnetic components of Fe-Ni Invar alloys disappear, and, at the same time, the peculier small thermal expansion disappeared. This effect of hydrogen was interpreted in terms of 3d hole filling with electrons transferred from hydrogen induced by the interaction between the metal and hydrogen as mentioned before.[35-37] However, the local environmental effect by interstitial hydrogen to change the magnetic state of nearby metal atoms

has not always been clarified by quantitative experiments. For the environmental effect of interstitial carbon atoms on the matrix atoms not for the fcc but for the bct martensite phase of Fe-C,[16,50] Fe-Ni-C[51] and Fe-Mn-C[17] alloys, Fujita et al. have precisely studied by means of Mössbauer effect, as mentioned before as well.

In the present chapter, Mössbauer spectra of carburized fcc Fe-Ni Invar and non-Invar alloys are shown and the precise spectral analysis is done. The change of Mössbauer spectrum of hydrogenated Invar alloy is also measured as a function of hydrogen concentration. The disappearance of weak ferromagnetic components influenced by interstitial solute atoms is discussed on the basis of the electron theory. The magnitude and range of influence of carbon to the magnetic properties in fcc Fe-Ni alloys are compared with those of hydrogen. Moreover, the crystal structure dependence of the effect of interstitial carbon on magnetic properties in fcc and bcc Fe-Ni alloys is discussed.

§2. Experimental Procedures

2.1 General procedures

The specimens of carburized and hydrogenated fcc Fe-Ni alloys were prepared as mentioned in the last chapter, where the final thickness of the specimen foils was 30μm and the radius was 1.00cm.

Mössbauer effect measurements were done at 77K by using the transmission method with the 14.4 KeV γ-ray radiations of

^{57}Fe from a 30 mCi ^{57}Co source dissolved in metallic rhodium. The block diagram of the apparatus is shown in Fig. 6.

The concentration of carbon was controlled to be 1.5 at.% in all carburized alloys and checked by X-ray measurement of the lattice constant as is shown in the last chapter.

The change of Mössbauer spectrum as a function of hydrogen concentration was obtained with one specimen by repeating the outgassing process of the heavily hydrogenated specimen at 30 °C in a glycerine and triethilenglycol mixture bath for 30 to 1000 mins. The measurements of Mössbauer effect and X-ray diffraction were repeated at 77K during the outgassing process. The amount of absorbed hydrogen was measured by collecting the released gas.

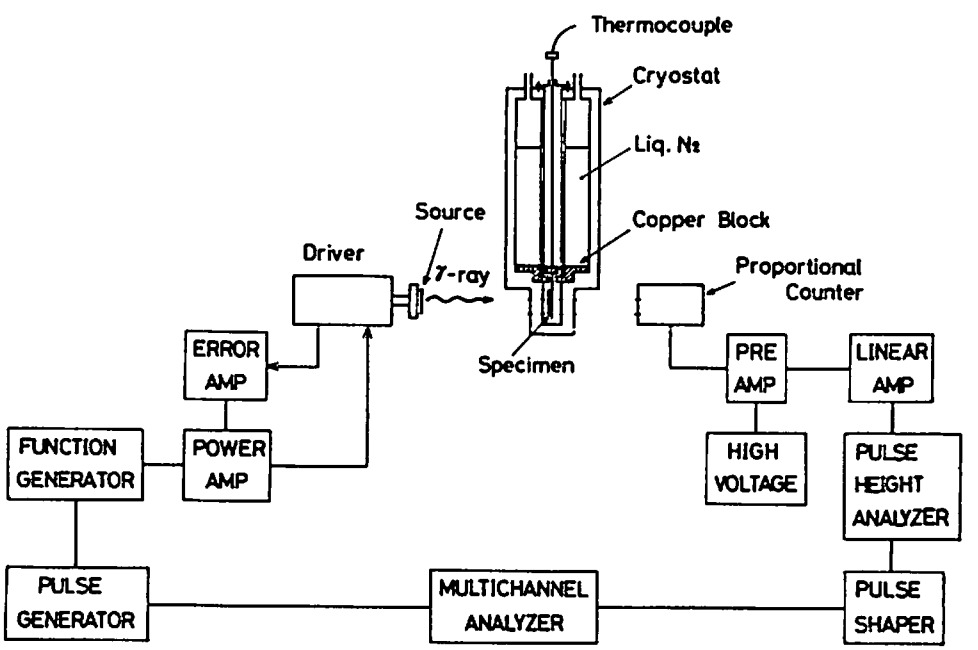

Fig. 6 Block diagram of Mössbauer measurement.

2.2 Brief description of Mössbauer effect and its applications[67-69)]

The recoil free emission and resonance absorption of γ-rays is called the "Mössbauer effect", which is discovered and explained by R. L. Mössbauer in 1958. If the recoil energy, E_R, associated with emission of γ-ray from a nuclei embedded in solid lattice is much smaller than the binding energy, E_B, of the lattice, the probability for emission without recoil energy loss, $\exp(-E_R/E_B)$, is extremely large. When the environments of the absorber nuclei are just the same as those of the source nuclei, sharp resonance absorption of the emitted γ-rays will occur at the absorber nuclei. However, in general, the environments of the source and absorber nuclei are different from each other, and, therefore, the energy levels of nucleus of absorption are different from those of source, and resonance will not arise, if the energy width of γ-ray is extremely narrow. But, if the Doppler energy is adequately given between the two nuclei, the resonance will take place again. Immediately after that, the excited absorber nuclei will decay with the reemission and the process will be repeated. This is the basic principle of the Mössbauer effect.

The obtained Mössbauer spectrum is characterized mainly by three parameters, that is, the isomer shift, internal magnetic field and quadrupole splitting, which are summarized in Fig. 7 in the case of ^{57}Fe Mössbauer nuclei. The only 14.4 KeV γ-ray energy brings about the recoil free resonance,

which corresponds to the transition energy between the excited state with nuclear spin, 3/2, and the ground state, 1/2.

Isomer shift, δ, is observed as a displacement of the resonance peak on the Doppler velocity scale as shown in the figure, arising from the electrostatic interaction between a nucleus and all of the extra charges at the nuclear position. The formulation is given by the following expression,

$$\delta = 2/5\pi Ze^2\{|\Psi_{(0)}|_a^2 - |\Psi_{(0)}|_a^2\}(R_e^2 - R_g^2) \quad . \qquad (3.1)$$

$|\Psi_{(0)}|_i^2$ is the charge density at the nucleus in the source, s, and the absorber, a. R_e and R_g are the excited and ground= state nuclear radii, respectively, and, for the ^{57}Fe Mössbauer nucleas the value of $(R_e^2 - R_g^2)$ is negative.

When a nucleus with a spin of I is in a magnetic field, H, the 2I+1 fold degeneracy is removed with the permitted energy levels,

$$E_M = -g\mu_N H m_I \quad , \quad (m_I = I, I-1, \ldots -I), \qquad (3.2)$$

where μ_N and g are the nuclear magneton and the gyromagnetic ratio. In the case of ^{57}Fe, the energy splitting can be detected in a Mössbauer spectrum as six resonance lines which arise from the selection rule, $\Delta m_I = 0, \pm 1$, as shown in the figure. In general, the magnetic field at the nuclear position is induced mainly by the polarization of 3d-electrons of the Mössbauer probe atom. Small contributions by other nearby atoms' magnetic moments also exist. The internal magnetic field of α-iron is -330 kOe, and, hereafter, the minus sign will be omitted.

The quadrupole splitting shown in the figure is produced by the interaction between the nuclear quadrupole moment, Q, and the electrostatic field gradient, q, due to the surrounding charge density. The interaction energy, E_q, is given by

$$E_q = \frac{e^2qQ}{4I(2I-1)} [3m_I^2 - I(I+1)] \quad . \qquad (3.3)$$

Mössbauer effect has been widely applied to physical metallurgy in order to investigate the scientific and technical problems such as of interstitial alloys, ferromagnetic alloys, order-disorder alloys, precipitation, lattice defects and so on.

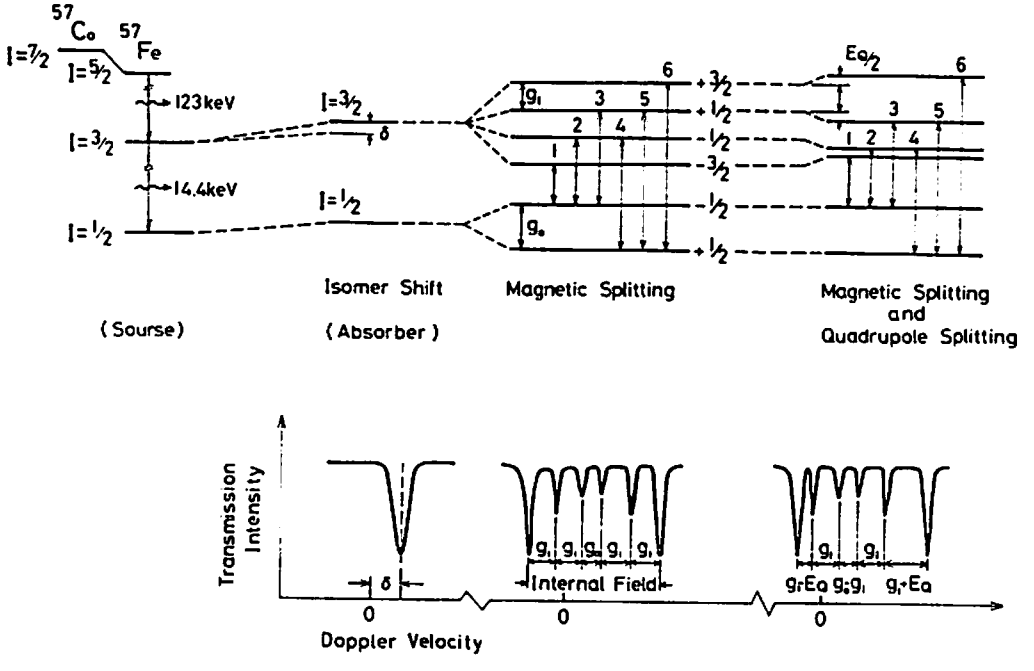

Fig. 7 Schematic description of Mössbauer effect. From the left hand side, decay schemes of ^{57}Fe in a sourse and the nuclear energy level of ^{57}Fe in an absorber for isomer shift, internal magnetic field and quadrupole field and corresponding Mössbauer spectra.

§3. Results and Analyses

3.1 Mössbauer spectrum of the Fe-33Ni Invar alloy as a referance

A Mössbauer spectrum of carbon-free Fe-33Ni Invar alloy is shown in Fig. 8(a). The six line absorption peaks come from the ferromagnetic iron atoms, which are broadened due to various environmental configurations around the iron atoms. The mean internal magnetic field measured by the peak-to-peak value is 335 kOe, and the isomer shift is 0.05 mm/s relative to pure iron. While, the quadrupole splitting was not observed in the spectrum. In addition to the normal ferromagnetic components, the spectrum has the characteristic weak ferromagnetic components corresponding to a wide spread dip of the spectrum from the base line, which is essencially different

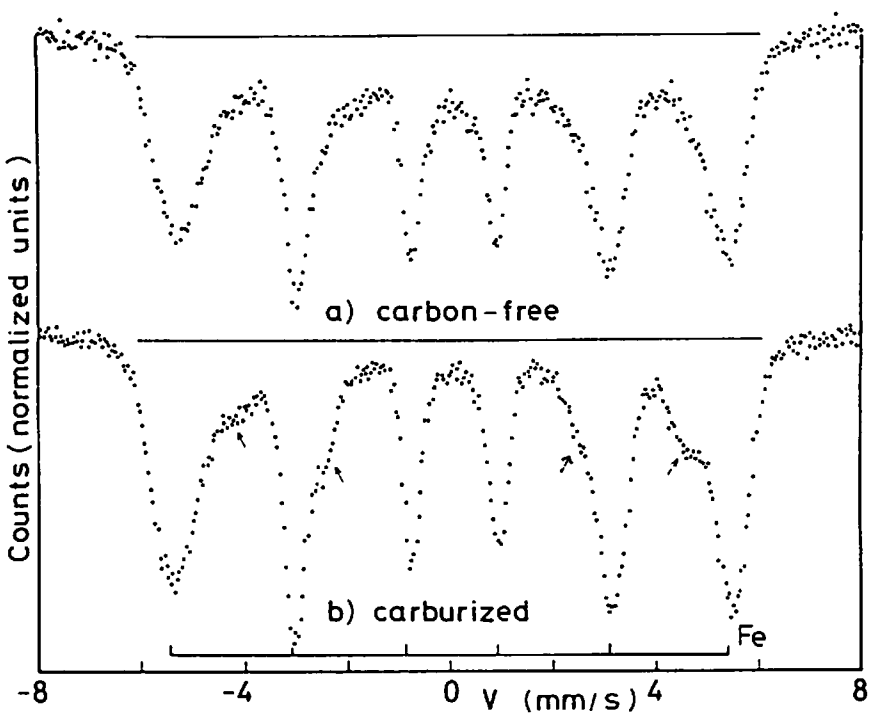

Fig. 8 a) Mössbauer spectrum of Fe-33Ni alloy at 77K before carburization.
b) The spectrum of the same alloy after carburization to 1.5 at.% carbon.

from the parabolic dip of the base line arising sometimes from an inadequate geometry of the apparatus.[67-69] The internal field distribution containing strong and weak ferromagnetic states will be visualized by the following technique of spectral analysis. By carburization, the spectrum shows noticeable changes due to the effect of solute carbon, as are seen in Fig. 8(b), which will be precisely described later.

The method of analysis to obtain the distribution function of internal field in an observed Mössbauer spectrum has been proposed first by Window.[70] In a ferromagnetic Mössbauer pattern, the sextet spectral component of each probe iron atom in each different environment can be characterized by three parameters, isomer shift, internal magnetic field and quadrupole splitting. In order to obtain the distribution function, it is first assumed that the spectrum consists of a number of Lorentz functions whose intensity distribution curve $P_{(E)}$ is given by the Fourier decomposition

$$P_{(E)} = \sum_{n=1}^{N} a_n f_{n(E)} , \qquad (3.4)$$

$$f_n(E) = \cos n\pi \frac{E - E_{min}}{E_{max} - E_{min}} - (-1)^n , \qquad (3.5)$$

where a_n is an amplitude of n-th component, E is the Doppler energy, and E_{max} and E_{min} are the maximum and minimum value of distribution adequately chosen by taking account of the experimental data. In the present analysis, the optimum

number of the function f_n is found to be six. Then we can easily compose the expected spectrum using the equation,

$$y_{fit}(E) = \sum_{k=1}^{31} \frac{P_{(E)}(\Gamma)^2}{(E-E_k)^2 + (\Gamma)^2} , \qquad (3.6)$$

where Γ is the half width of each Lorentz function. In the present case, the region $E_{min} \leq E \leq E_{max}$ is divided into 30 elements with equal separations. The values of the coefficients, a_n's in eq. (3.4), are determined by the least-square mean analysis,

$$d^2 = \sum_{I=1}^{MCH} (y_{data}(I) - y_{fit}(I))^2 , \qquad (3.7)$$

where I is the data points, i.e., channel numbers of the multichannel analyzer. Thus employing the above analytical method, we can obtain the distribution function of internal field in the specimen.

According to the above method, the internal magnetic field in the Mössbauer spectrum of the Invar alloy is obtained and showed by the solid line in Fig. 9, and the best fit curve for the original spectrum is given by the solid line in Fig. 10(a). The obtained distribution function in Fig. 9 indicates that 70 % of the iron atoms in the Fe-33Ni Invar alloy are in the strong ferromagnetic state and about 30 % in the weak ferromagnetic state. The boundary between the two states is shown by a dot-dash-line in Fig. 9.

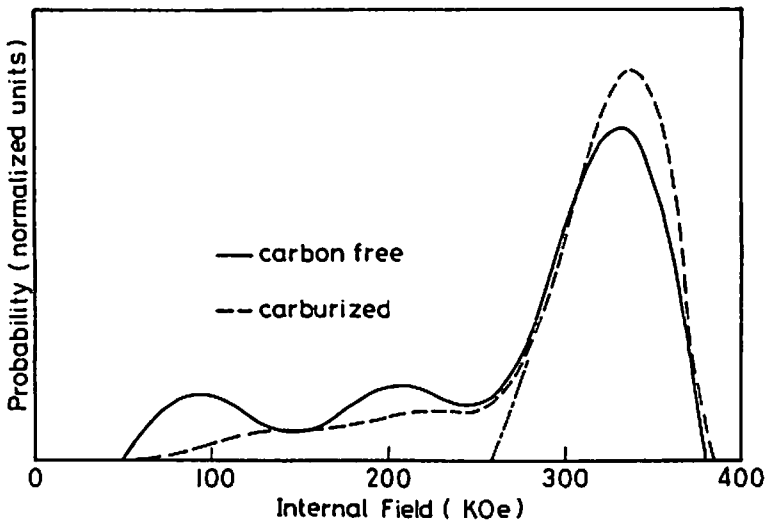

Fig. 9 Analytical curves of the internal magnetic field distribution. Solid and broken line are of the Fe-33Ni alloy at 77K before and after carburization, respectively.

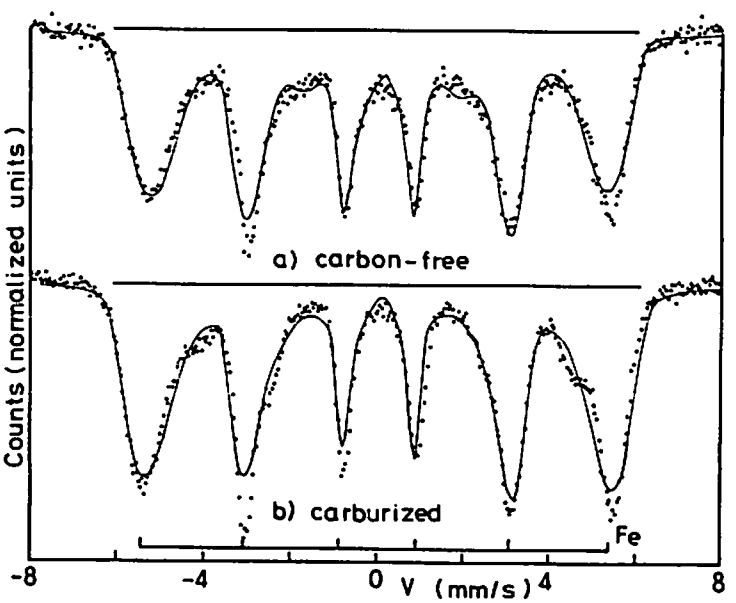

Fig. 10 Best fit curves for the originel spectra in Figs.8 (a) and (b).

3.2 Mössbauer spectrum of Fe-33Ni-C alloy and analysis

By carburization, the Mössbauer spectrum of the Fe-33Ni Invar alloy changed as shown in Fig. 8(b). Comparing this spectrum with the carbon-free one, the dip from the base line becomes shallower, showing a reduction of the weak ferromagnetic components, which is similar to that observed in the case of hydrogenation of Invar alloys.[35-37] According to the analysis of the internal magnetic distribution in the carburized system, the distribution curve shown by the broken line in Fig. 9 and the best fit synthesized spectrum of Fig. 10(b) are obtained, and it turns out that the fraction of the weak ferromagnetic components decreases from 30 % to 15 %. This means that a half of the weak ferromagnetic components of the carbon-free alloy is affected by 1.5 % carbon and becomes strong ferromagnetic.

In addition to the above change, some small shoulders appear on the broad ferromagnetic six lines, for instance, on the inner side of the leftest, the second left and the rightest peak in Fig. 8(b), as indicated by small arrows. This change was supposed to be due to interstitial solute carbon, because the shoulder peaks do not correspond to any carbide structure, and the X-ray measurements show no trace of precipitation of new phases.

Since the concentration of carbon in the alloy is relatively low, the observed Mössbauer spectrum in Fig. 8(b) will be composed of the carbon-affected and unaffected parts.

As mentioned before, the weak ferromagnetic part partially

into strong ferromagnetic part by carburization. The fact makes it possible to separate the above spectrum into two part. The separation of the spectral components was done by subtracting 50 % of the normalized total intensity of the carbon-free spectrum in Fig. 8(a) from the carbon-affected spectrum in Fig. 8(b), since a half of metal atoms was supposed to be affected by carbon and the other half unaffected, as mentioned before. The result of subtraction, corresponding to the carbon-affected part in the original carburized spectrum, is shown in Fig. 11(a). The subtracted spectrum consists of two sub-components, that is, six line components, M_A, the peak positions of which are very slightly wider than those of the original main peaks in Fig. 8(a), and an additional smaller and less spread six line components, M_B, which is no other than the sub-shoulders in the original carburized spectrum in Fig. 8(b). Decomposition of the two sub-components was successfully done by calculating the components M_A by using the necessary parameters, such as the line positions, half width, intensities, and line shape, which were estimated and modified from the original carbon-free spectrum in Fig. 8(a). The calculated profile of M_A is shown in Fig. 11(a) by the solid line and the separated profile M_B is given in Fig. 11(b). The internal magnetic fields of M_A and M_B are 340 kOe and 269 kOe, respectively, and their isomer shifts are 0.07 mm/s and 0.24 mm/s relative to pure iron. The integrated intensity ratio, M_B/M_A, is 0.24, and, therefore, the reduced fraction of the above components

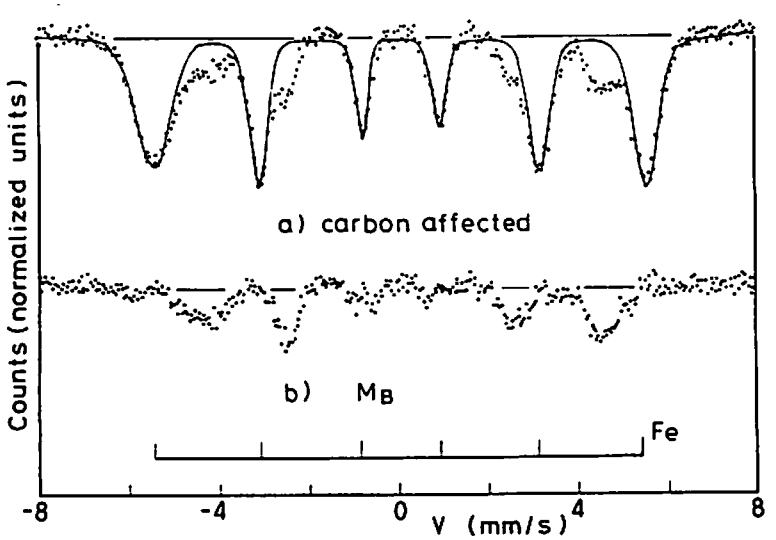

Fig. 11 a) The remnant spectral component after subtraction of 50% of the spectrum in Fig. 8(a) from Fig. 8(b), corresponding to the carbon affected part in the latter spectrum. The spectrum, (a), is further decomposed into the sub-components, M_A and M_B. The latter, shown in the figure (b), is concluded to arise from the iron atoms first-neighbouring with the interstitial carbon, and the former, shown by the solid line in (a), from the second and third neighbour ones.

in the original carburized spectrum in Fig. 8(b) can be obtained. The fraction of M_A is about 0.40, that of M_B is about 0.10, and that of the carbon-unaffected component is about 0.50. No detectable quadrupole effect appeared in the observed spectra as well as in their analized components.

For the assignment of the spectral components and the estimation of the effect of carbon on the nearby iron atoms, a statistical calculation based on the binominal distribution in the near neighbour configurations was applied. The

probability of finding n_j's (j=1,2,.., k) interstitial carbon atoms in the j-th shells around a central iron probe atom is

$$P_{(n_1,n_2,\ldots,n_k)} = \prod_{j=1}^{k} {}_{y_j}C_{n_j}\, c^{n_j}(1-c)^{y_j-n_j}, \quad (3.7)$$

where y_j is the number of octahedral interstices in the j-th shell in the fcc lattice.[71] The carbon concentration, c, is 0.015 in the present case. According to the above formula, the probability of finding any carbon in the first shell,

$\sum_{n_1\neq 0} P_{(n_1,0,0)}$, is 0.087, that within the first and second shell $\sum_{n_1+n_2\neq 0} P_{(n_1,n_2,0)}$=0.191, and within the third and inner shells, $\sum_{n_1+n_2+n_3\neq 0} P_{(n_1,n_2,n_3)}$ is 0.437.

In the above calculation, the effective shells where any carbon atom within the shells affects the central iron atom are assumed to be the third shells on the ground of the fact that a half of the weak ferromagnetic components in the carbon-free alloy becomes strong ferromagnetic by carburization to 1.5 at.% carbon as mentioned before and the fact that in the case of the bcc martensite structure of Fe-C, Fe-Ni-C and Fe-Mn-C alloys the effect of the interstitial carbon atom extends over the third shell atoms.

Comparing the experimental values, M_B=0.1, M_A=0.4 and the remainder part in the carburized spectrum=0.5, with the above

calculated values, a satisfactory explanation of fractional intensitities of the spectral components and their assignment are obtained as follows: The component M_B arises from the ^{57}Fe atoms first-neighbouring with carbon atoms, which will correspond to the probability 0.087. The components M_A are due to the iron atoms affected by the second- and/or third-neighbouring carbon atoms, and the remainder part of the carburized spectrum comes from those with the fourth- and further-neighbouring with carbon and thereby unaffected, where their fraction must be 0.350 (=0.437-0.087) and 0.563 (=1-0.437), respectively, which are in good agreement with the experimental values, about 0.4 and 0.5, respectively. The calculated intensity ratio, M_B/M_A=0.25, is also very close to the experimental value, 0.24.

From the above analysis, it is concluded that the average value of the internal magnetic field of the strong ferromagnetic iron atoms, 335 kOe, in the Fe-33Ni Invar alloy is reduced by 20 %, or by 65 kOe, when first-neighbouring by an interstitial carbon atom, and is enhanced by 2 %, or by 6 kOe, when second- or third-neighboured by carbon.

3.3 Spectral analysis of other Fe-Ni-C alloys

In the case of an Fe-64Ni non-Invar alloy which has no weak ferromagnetic components, peak shoulders by carburization are also detected on the Mössbauer spectrum. Figures 12(a), (b), (c) and (d) show the carbon-free spectrum, carburized

spctrum, subtracted spectrum with the calculated components M_A, and the final remnant spectrum M_B, respectively. The procedure to obtain the calculated spectra is the same as that used for the above mentioned Invar and the result of the analysis is essentially the same, that is, the fraction of M_B is about 0.1, that of M_A about 0.4, and the remainder about 0.5.

The internal magnetic field of probe iron atoms affected by carbon in Fe-64Ni non-Invar alloy also shows quite similar behaviour to that in Fe-33Ni Invar alloy as mentioned in the last section. Moreover, this is in accordance with what has been observed on the bcc martensite structure of Fe-C,[16,50] Fe-6Ni-C[51] and Fe-3Mn-C[17] steel. The average values of the internal magnetic field of various components in the fcc Fe-33Ni-C and Fe-64Ni-C alloys are plotted against the near neighbour iron-carbon distance in Fig. 13 together with the bcc Fe-6Ni-C alloy.[51]

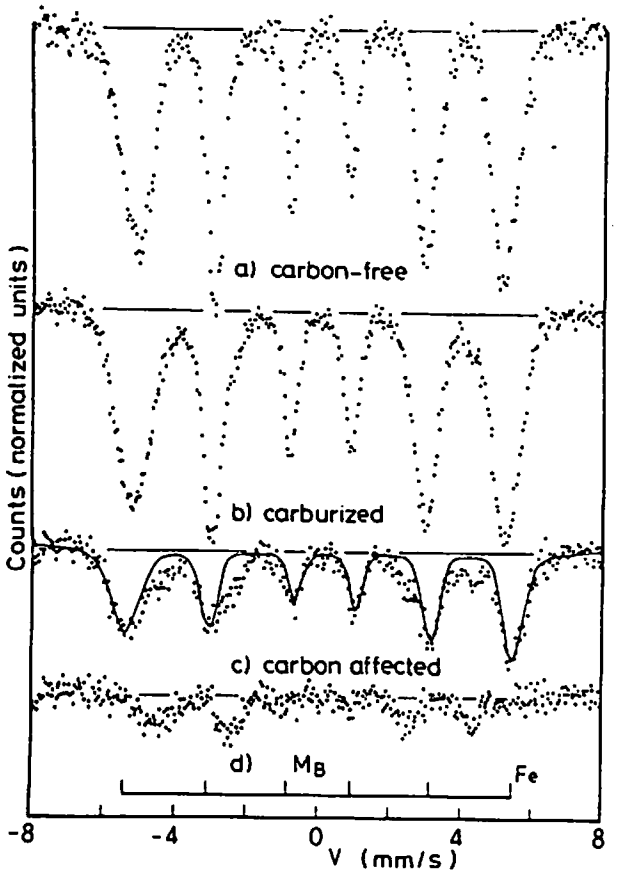

Fig. 12 Mössbauer spectra of Fe-64Ni alloy at 77K.

a) The carbon-free spectrum.

b) After carburization to 1.5at.%C.

c) The carbon affected part, where solid line is the calculated profile M_A.

d) The separated profile M_B.

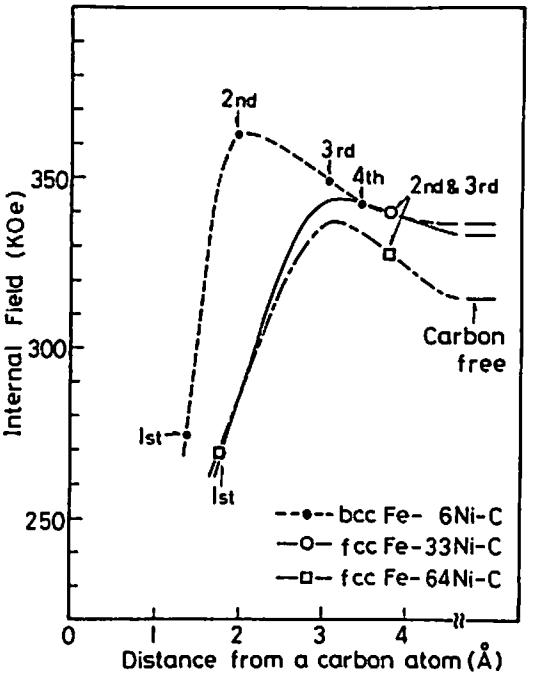

Fig.13 Variation of internal field of iron atoms with the iron-carbon distances in the fcc Fe-33Ni-C, fcc Fe-64Ni-C and bcc Fe-6Ni-C alloys.

3.4 Mössbauer spectrum of Fe-33Ni-H solid solution alloys

Typical Mössbauer spectra of Fe-33Ni-H solid solution alloys are shown in Figs. 14(b), (c), (d), (e) and (f) with the hydrogen-free one in the figure (a), where the amount of absorbed hydrogen in the specimens were controlled so as to have various concentrations in the hydrogen solid solution range. The weak ferromagnetic components rapidly disappear by an addition of small amount of hydrogen, as well as in the case of carburization, but no remarkable sub-shoulders are observed on the main peaks.

The hydrogen concentration dependence of the internal magnetic field, the isomer shift and the reduction of the weak ferromagnetic components are summarized in Fig. 15. The values of internal magnetic field and isomer shift were determind from the peak positions of the ferromagnetic six line spectra. The former linearly increases with the increasing hydrogen concentration until 5 % hydrogen and then linearly decreases, exhibiting a maximum like the Slater-Pauling curve and the latter changes in proportion to the hydrogen concentration. The amount of the weak ferromagnetic components was evaluated from the depth of the dip from the base line in a spectrum, which was checked by the calculation of the internal field distribution function by the Fourier analysis as mentioned before. The components decrease in proportion to the hydrogen concentration until 5 % hydrogen, and, at that concentration, they disappear completely as shown

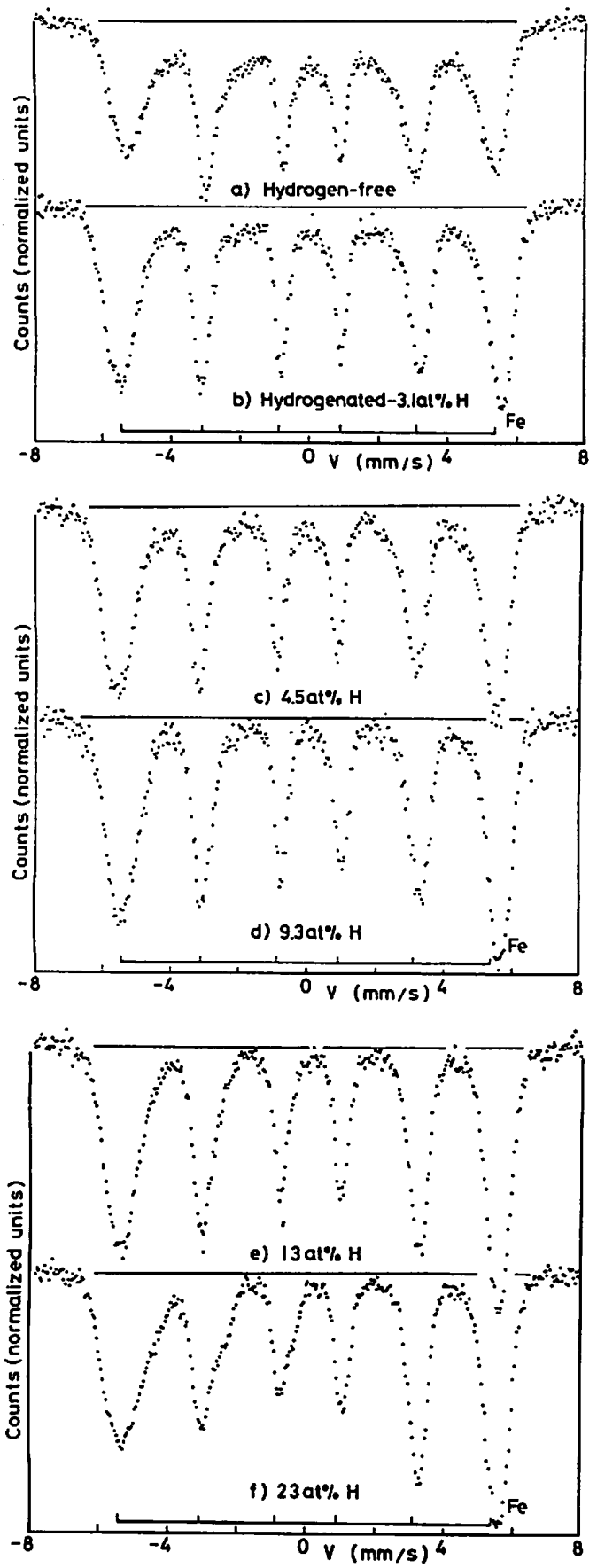

Fig. 14 Typical Mössbauer spectra of hydrogenated Fe-33Ni alloys.

a) Hydrogen-free.

b) Hydrogenated to 3.1at.%H (H/M=0.03)

c) 4.5at.%H (H/M=0.05)

d) 9.3at.%H (H/M=0.10)

e) 13.0at.%H (H/M=0.15)

f) 23.0at.%H (H/M=0.30)

by the lowest curve in Fig. 15. According to the before mentioned analysis using the binomial distribution relation, this means that the effect of an interstitial hydrogen atom on the weak ferromagnetic iron reaches the second- to third-neighbouring atoms around it.

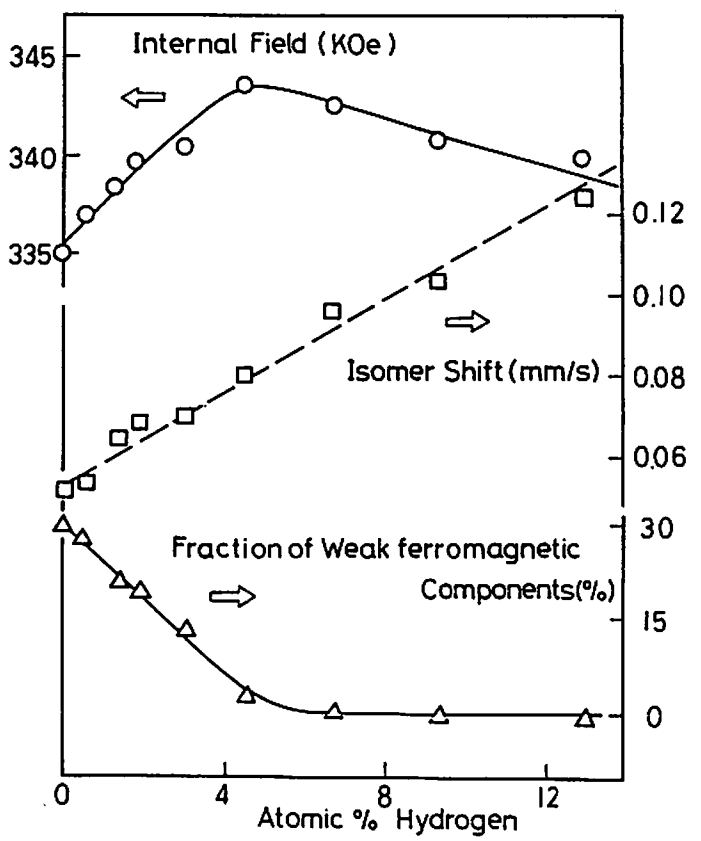

Fig. 15 The values of the internal magnetic field, the isomer shift and the fraction of the weak ferromagnetic components of the Fe-33Ni-H alloy against the hydrogen concentration.

§4. Discussion

4.1 Conversion from weak to strong ferromagnetism by interstitial elements

The disappearance of weak ferromagnetic components of Fe-Ni Invar alloys by hydrogenation was found by Sohmura and Fujita for the first time as mentioned before.[35-37] Based on the recent theoretical results calculated by Adachi et al.[42,52] using a DV-Xα cluster method, they have interpreted the effect of interstitial hydrogen in such a way that hydrogen-induced bonding levels and anti-bonding levels would be formed by the hybridization of hydrogen's 1s and metal's 3d states mainly and accordingly the deformation of band structure and the electron redistribution would result in the filling up of the up spin holes of the 3d state, and, therefore, the disappearance of the weak ferromagnetism. A similar molecular orbital calculation was applied to various transition metal-carbon clusters,[42] and similar hybridization of orbitals inducing new energy levels and electron redistribution was predicted.

Apart from the above discussion, it must be noted that the disappearance of weak ferromagnetism by the interstitial additives is different from the gradual change of internal magnetic field such as the gradual peak shifts in the ferromagnetic spectrum as are seen in Fig. 14. On the contrary, when the iron atoms with the weak ferromagnetic state are affected most likely by the first- to the third-neighbouring interstitial atoms, they drastically change to the strong

ferromagnetic ones. This suggests that the weak ferromagnetic state is less stable in Invar alloys and can be easily turned into the strong ferromagnetic states by an addition of a little amount of transferred electrons from the interstitial atoms. After the transition from the weak to strong ferromagnetic state, one can not differenciate between the component which was strong ferromagnetic from the begining and that which was originally weak ferromagnetic in the Mössbauer spectrum.

As was shown in the last chapter, the difference of the amount of hydrogen absorption between Invar and non-Invar alloys was not found. This is readily understood from the fact that the characteristics of Invar are lost by an addition of a few percent of hydrogen.

4.2 Environmental effect of interstitial carbon and hydrogen in fcc Fe-Ni alloys.

4.2.1. The magnitude and range of influence of interstitial atoms to the magnetic states of host metal atoms

As perceived in Fig. 13, the value of the ferromagnetic internal field of an iron atom is reduced as much as by 20 % by a first-neighbouring interstitial carbon atom, while the value is enhanced by a few percent by a second- or third-neighbouring carbon atom, which seems to be quite common among the iron based alloys irrespective of fcc or bcc structure.

The average internal field of Fe-33Ni-H alloys decreases with increasing hydrogen concentration beyond 5 %, as the uppermost curve in Fig. 15 shows. Although the separation of spectral components is not possible in the case of hydrogen solid solution, it is most likely that the decrease of internal magnetic field is due to the first-neighbouring hydrogen atoms. Nevertheless such an environmental effect of hydrogen to change the internal field must be considerablly smaller than that of carbon; a crude estimation from the curve in Fig. 15 gives that the amount of reduction of internal magnetic field by the first-neighbouring hydrogen atom would not exceed 10 kOe, that is, the slope of this curve, 2.8kOe/5at.%, and the mean number of hydrogen atoms occuping at first-neighbouring octahedral interstices,0.27numbers/5at.%H by the binominal calculation, give the value, 10kOe/number(= 2.8/0.27), and that by the second-neighbour would be negligibly small.

The mechanism of such a reduction or enhancement of internal field by interstitial elements has been theoretically interpreted. According to the before mentioned DV-Xα cluster calculation,[42,43,52] the magnetic moment of an iron atom first-neighbouring with an interstitial carbon atom in the bcc martensite lattice to be reduced by a few tens percent due to the transferred electron between the carbon atom and surrounding metals giving rise to the increase of Fermi level. Although a slight increase of the 3d moment of the second-neighbouring iron atoms has not always been clarified theoretically, it may

be explained by the redistribution of a small amount of transferred electrons in a second-neighbouring iron's 3d shell. That is, in an iron's 3d-shell which has a slight hole in the up spin band and a large amount of hole in the opposite band in pure iron[72] and Fe-Ni alloys,[73] transferred electrons may preferentially occupied in the up spin band's hole because of intra-atomic coulomb and exchange interactions.[74] In practice, the resonance spectrum of NMR of carburized cobalt which has no hole in the up spin band shows that the internal field by second- and third-neighbouring with carbon is smaller than the unaffected one.[23]

4.2.2. The crystal structure dependence of the effect of carbon on magnetic states in fcc and bcc Fe-Ni alloys

It looks strange that the environmental effect of interstitial carbon in the bcc martensite structure and in the fcc Fe-Ni alloys exhibit nearly the same behaviour as shown in Fig. 13. The lattice constants and near neighbour configurations, which strongly influence the formation of covalent bonding and other local electron distributions, are fairly different in the two structures. For instance, the octahedral interstitial site in the bcc structure is first-neighboured by two host metal atoms about 1.44 Å apart and second-neighboured by four about 2.03 Å apart, while that in the fcc structure is surrounded by six metal atoms equally distance by 1.81 Å, if the local lattice relaxation due to interstitialcy is not taken into account. However, the first nearest distance in

the bcc lattice is actually expanded so that the carbon atom can be squeezed into the irregular-octahedral interstice, and this makes the second nearest distance shorter, as are well known in the study of tetragonality of martensite structure of steel.[16,17,51,52] Therefore, the nearest neighbour distances in the two structures will not be so different as above mentioned, and, in addition, the azimuthal relation ship between the metals' d-orbitals and carbon's s- and p-orbitals will become more or less the same. For these reasons, the same behaviour and nearly the same order of magnitude of the environmental effect of interstitial carbon in the two structures could be expected.

4.2.3. Isomer shift and lattice distortion by interstitials

The isomer shift of the fcc Fe-33Ni alloy is 0.05 mm/s relative to pure iron and that of the carbon-first-neighbouring iron atom in the same alloy is 0.24 mm/s. That is, the isomer shift change by the first-neighbouring carbon in this alloy is 0.19 mm/s, which is considerably larger than that in the bcc Fe-C alloy, -0.03 mm/s.[16,50] When a carbon atom is in an octahedral interstitial site, the atomic volume of nearby iron atoms will decrease. The volume dependence of the isomer shift of iron has been first estimated by Ingalls[75] using Stern's modified tight-binding method.

According to his calculation, the 4s electron density at the nucleus will increase with decreasing atomic volume, giving rise to a negative isomer shift change, which can be

evaluated by $\Delta\delta \simeq \alpha(\Delta V/V)$, where $\Delta\delta$, ΔV and V are isomer shift change, volume change and atomic volume, respectively, and the value of α is about 0.8 mm/s for fcc structures and 1.4mm/s for bcc ones. Comparison between the radius of octahedral interstices of the both structures, 0.19 Å for bcc and 0.53 Å for fcc, and the Goldsmith radius of carbon, 0.77 Å,[23] shows that the iron atoms first neighbouring with carbon in the bcc alloy is more squashed than those in the fcc alloy, and ΔV is evaluated to be -0.94 Å for bcc Fe-C alloy and -0.22 $Å^3$ for fcc Fe-33Ni-C alloy. Therefore, $\Delta\delta$ is calculated to be -0.11 mm/s for bcc Fe-C alloy and -0.01 mm/s for fcc Fe-33Ni-C alloy, where the atomic volume is 11.7 $Å^3$ and 12.1 $Å^3$, respectively. Another impotant contribution to the isomer shift comes from the covalent bonding between the carbon and iron atoms. The internal magnetic field of the first-neighbouring iron in the bcc and fcc alloys is considerably smaller value than that in carbon-free alloys, and, therefore, the isomer shift change of the iron atom will be a positive and more or less the same value because of the increase of 3d-electrons and the same values of internal field of the iron in the both alloys. On the other hand, the contribution of 3d electrons to the change of isomer shift arising from the volume change was found to be very small. Therefore, in a qualitative discussion, the more negative isomer shift of the first-neighbouring iron atoms in the bcc Fe-C alloy than in the fcc Fe-Ni alloys is due to the volume change effect.

The isomer shifts of the iron atoms second- and third-

neighbouring with carbon in both fcc and bcc alloys are about +0.07 mm/s. This slight increase could be interpreted by the increase of the 3d electrons of these iron atoms as mentioned before.

Chapter 4. Thermal Analysis of Hydrogen Outgassing Process of Pd-H, Ni-H and fcc Fe-Ni-H Alloys

§1. Introduction

In the last chapter, the local electronic structure of a host atom around a hydrogen atom in fcc Fe-Ni alloys was investigated by means of Mössbauer effect and the electronic change by hydrogenation was explained in terms of the formation of the bonding level between metal and hydrogen atoms and the increase of Fermi level due to the transferred electrons induced by the above bonding formation. The above changes must strongly affect the stability of hydrides and the solubility of hydrogen in metals. In practice, in chapter 2 we suggested that the d-electron configuration of the matrix atoms played an important role on the bonding between the metal and hydrogen atoms.

The stability of hydrogen in metals is another important factor necessary to describe the state of hydrogen, and it corresponds to the interaction energy of the whole metal-hydrogen system including the lattice distortion energy, which can be measured quantitatively by a technique of thermal analysis such as the differential thermal analysis (DTA) or differential scanning calorimetry (DSC). In the present study, we have measured the heat of reaction for the hydrogen outgassing process of Pd-H, Ni-H and fcc Fe-Ni-H alloys by means of DSC. The observed dissociation energy as a function of hydrogen concentration was interpreted semiquantitatively

in terms of the lattice strain energy and electronic interaction energy of the metal-hydrogen systems, and the main factor of the energy change due to the hydride formation in metal was discussed.

§2. Experimental Procedure in Differential Scanning Calorimetry (DSC)

The hydrogenation of palladium, nickel and fcc Fe-Ni alloys was done by using the same condition as mentioned in chapter 2. The charged specimen was punched out in liquid nitrogen and a round plates with the diameter of 6.0 mm and the thickness of 30 μm were formed.

Thermal analysis was done by using the Du Pont model 990 differential scanning calorimeter with a pressure DSC cell at a heating rate of 5°C/min or 10°C/min. The chamber was evacuated in order to avoid extra chemical reactions on the active surface of the specimen. The block diagram of the apparatus is shown in Fig. 16. When heat of reaction is evolved in a specimen,

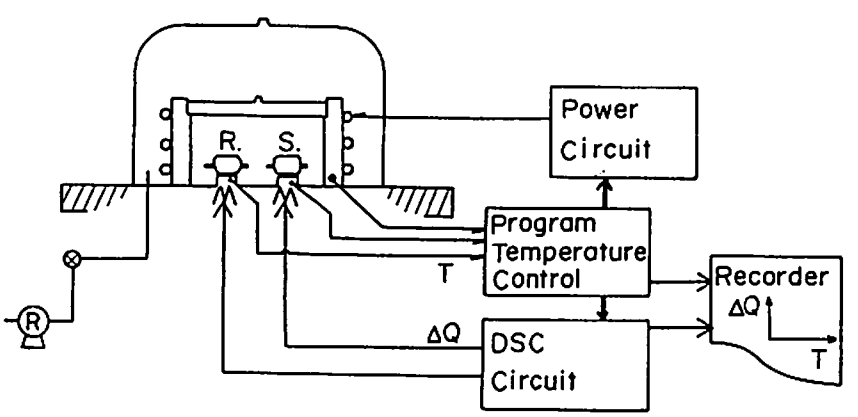

Fig. 16 Block diagram of differential scanning calorimetry (DSC).

the temperature difference appears between the specimen and the reference. At this instance, the balancing heat power to make the temperature difference zero is supplied to the specimen or the reference, which just corresponds to the heat of reaction occurred in the specimen. The balancing heat power is measured by the electric current of the heater. A sample capsule in the figure contained a hydrogenated specimen weighing about 30 mg. The calibration of the instrument was performed by the melting of indium and tin.[76,77)]

X-ray diffraction measurements were carried out at room temperature by using Co-Kα radiation. The amount of absorbed hydrogen was measured by the gas volumetric method in a vacuum cell as shown in Fig. 3.

§3. Results and Analysis

3.1 The outline of experimental results and analysis

When the specimen was hydrogen-free, the DSC curve was completely flat, exhibiting neither exothermic nor endothermic reaction. On the other hand, the hydrogen outgassing process appeared as an upward or downward deviation from the base line, which corresponded to the exothermic or endothermic reaction, respectively. In the outgassing process, atmosphere condition was very important. In the case of Pd-H alloy, as shown in Fig. 17(a), an exothermic reaction process was observed in air, as in the ordinary DSC measurement. However, it was remarkably reduced in a flowing nitrogen or

argon atmosphere and, further, it was completely changed into an endothermic reaction when the apparatus was evacuated to 1000Pa or lower as shown in figs. 17 (b), (c) and (d). This suggested that the exothermic reaction was due to extra chemical reactions between hydrogen and oxygen gas on the surface of palladium. In this experiment, therefore, it was decided to do the measurements under a vacuum of 1 Pa. In this vacuum condition, the DSC curves were delayed to appear by about 40 degrees, but, otherwise, the measurements were quite stable and reproducible. When the heating rate was changed from 1°C/min to 20°C/min, the exo- and endo-thermic peaks shifted to the higher temperature side by the order of several tens degrees, but the profile of the DSC curve was essentially not changed. When the hydrogen concentration in the specimen was changed, the peak shift was observed, and, at the same time, the DSC profile changed.

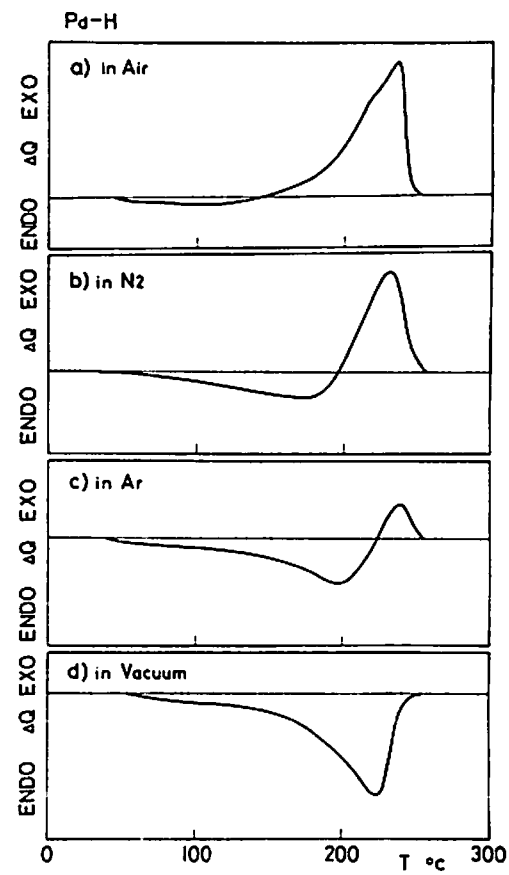

Fig. 17 The change of the DSC curves of hydrogen outgassing process of Pd-H alloy in verious atmosphere conditions.
a) in air.
b) in a flowing neitrogen gas (flow rate 7mℓ/min.)
c) in a flowing argon gas (flow rate 7mℓ/min.)
d) in a vacuum of 1000Pa.

Figures 18 (a), (b) and (c) show typical DSC curves of hydrogen outgassing process of Pd-H, Ni-H and Fe-33Ni-H alloys,

respectively. In the broad sense, the dissociation temperature becomes lower in the order of palladium, nickel and iron-nickel alloy, while the peak area per mol of released gas, i.e., the heat of dissociation becomes larger in this order. The above order is also valid for the stability of the hydride.[78] Generally speaking, an endothermic reaction was found in the dissociation of stable hydride such as palladium hydride, and an exothermic one was observed in the case of the dissociation of unstable hydride.

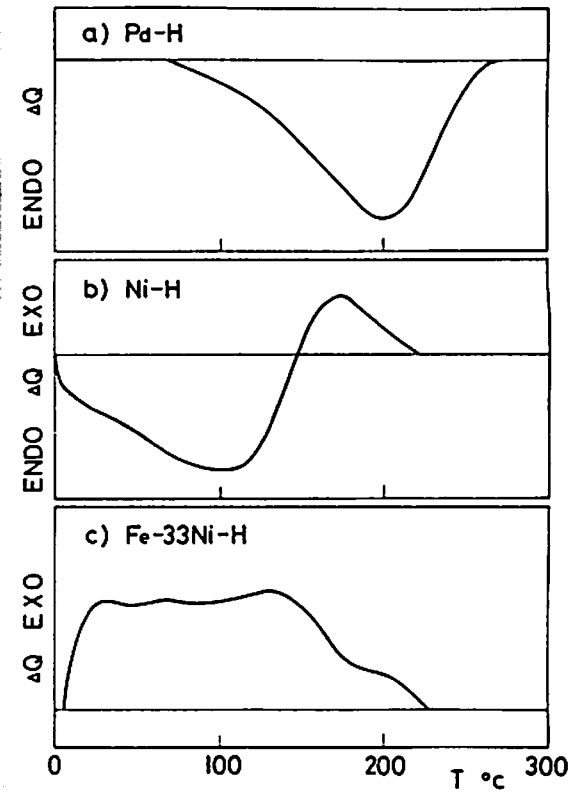

Fig. 18 a) A typical DSC curve of Hydrogen outgassing process of Pd-H alloy.
b) A DSC curve of Ni-H alloy.
c) A DSC curve of Fe-33Ni-H alloy.

In order to investigate the gradual reaction process in details, hydrogen outgassing process of each specimen which was hydrogenated with the same condition was stopped at certain temperature in the course of heating, and, immediately the sample was taken out and cooled down to the room temperature, and the X-ray diffraction pattern and the residual amount of absorved hydrogen of each sample was measured. From the difference in the total heat of reaction and amount of residual hydrogen between two measurements, the differential heat of reaction was obtained.

3.2 DSC of hydrogen outgassing process of Pd-H alloys

Figure 19 (a) shows the DSC curve of a Pd-H alloy, in which the arrest temperatures are indicated by small arrows, and the residual amount of absorved hydrogen at these temperatures are shown by open circles in Fig. 19(b). The absorved or released amount of heat between two successive temperatures, ΔQ, as indicated by hatching in Fig. 19(a), divided by the amount of released gas, Δn, as shown in Fig. 19(b), gives the differential heat of reaction. For the evaluation of the dissociation energy between hydrogen and metal, the integral representation of the differential heat of reaction is useful. The integration is done from each arrest temperature to the end of the reaction and it is divided by the amount of released gas in the same range, i.e.,

$$\frac{\int_0^n \frac{\Delta Q}{\Delta n}\, dn}{\int_0^n dn} = \frac{Q}{n} . \qquad (4.1)$$

The heat of dissociation, Q/n, was obtained as a function of hydrogen concentration at each step, as shown by open circles in Fig. 20. On the other hand, the value, Q/n, could be also found from the total sum of the peak area of the DSC curve for each specimen. Six full dots in the figure were thus obtained from six specimens with different hydrogen concentration. The broken line in Fig. 20 means the two phases region, where β-hydride and α-hydrogen solid solution coexist. It was estimated by combining the X-ray measurements, the phase

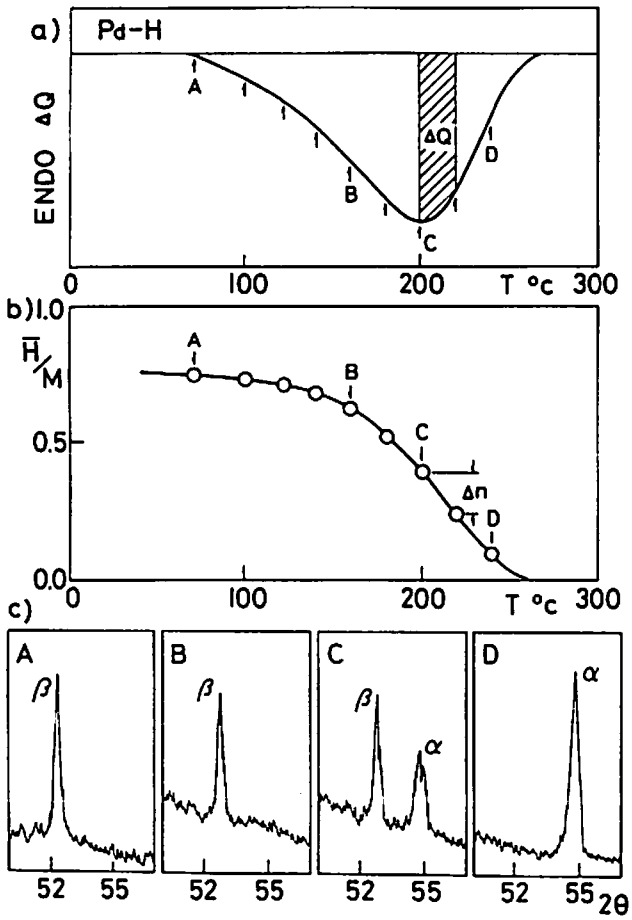

Fig. 19 a) DSC curve of hydrogen outgassing process of Pd-H alloy. The amount of hydrogenated specimen is 23.8mg and the hydrogen metal ratio, H/M, is 0.75. The heating rate is 10°C/min. The total heat of the process, Q, is -4.6J. Small arrows indicate the temperatures where the measurement was stopped and the specimen was taken out. b) Hydrogen concentration of the specimens which were taken out at the temperatures shown by arrows in the figure (a).

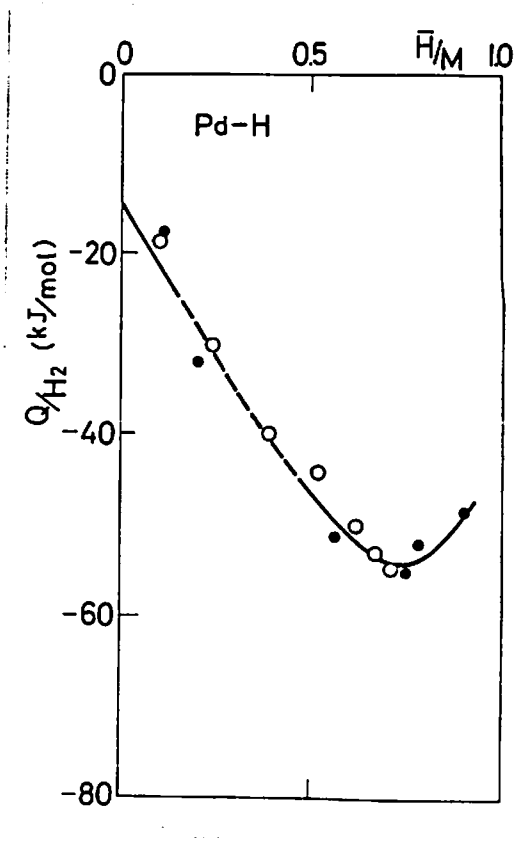

Fig. 20 Heat of dissociation for hydrogen outgassing process of Pd-H alloys as a function of the hydrogen concentration. Open circles mean the values which are evaluated by integrating the differential heat of reaction from each temperature to the end of the reaction and dividing it by the amount of released gas by using the results as shown in Figs. 19(a) and (b). Full dots indicate the values which are obtained from the total sum of the peak area of the DSC curves for six specimens with different hydrogen concentration. The broken line means the two-phase region.

diagram of Pd-H alloy,[8] and the path of the outgassing process shown in Fig. 19(b). Figure 19(c) shows typical X-ray diffraction patterns of the specimens, which had been heated up to the temperatures A, B, C and D indicated in the figure (a) and cooled down to the room temperature. The pattern C in the figure indicates the existence of the two phases. In this region, the curve of Q/n in Fig. 20 will follow the lever relation, in which the mean value of heat of reaction, $\bar{Q}$, is written by $\bar{Q}=q_\alpha n_\alpha+q_\beta n_\beta$, where q_i and n_i are the heat of reaction and fraction of i-phase. An anomalous behaviour which would indicate the difference between the two phases can not be detected in the thermal analysis as in Fig. 19 (a). In practice, the inherent difference between the two phases is little so far as the lattice constant, electrical resistivity and magnetic susceptibility,[1,2,23,79] which are continuously in proportion to the hydrogen concentration. Therefore, the plotted value of Q/n in the two phases region against average hydrogen concentration in Fig. 20 gives the mean value evaluated by using the lever relation. The heat of dissociation in Fig.20 increases with the decrease of hydrogen concentration. While, in the high hydrogen concentration region, the gradient of Q/n becomes positive as shown in Fig. 19. The positive gradient indicates that the hydride turns to be unstable state. In fact, the hydride of H/Pd=1.0 prepared at room temperature decomposes gradually till the concentration of H/Pd=0.7~0.8.

Under the present experimental condition of constant pressure, the heat of reaction, Q, is equal to enthalpy, H_{exp}. The curve of heat of dissociation in Fig. 20 is approximated by

$$\frac{H_{exp}}{\text{mol of } H_2} = \alpha - \beta n + \gamma n^2 \ \ldots, \qquad (4.2)$$

where α, β and γ are coefficients to be given by the experiment.

3.3 DSC of Ni-H and fcc Fe-33Ni-H alloys

In the case of Ni-H and Fe-33Ni-H alloys, H_{exp} per mol of H_2 is also expressed by the similar expansion form in eq. (4.2) with different values of coefficients. Figure 21(a) shows the DSC curve of Ni-H alloy, where small arrows indicate the points of sampling. The values of hydrogen concentration and X-ray profiles of specimens in the course of the process are shown in Figs. 21(b) and (c), respectively. Figure 22 shows the heat of dissociation for Ni-H alloy obtained through the same procedure as in the case of Pd-H alloy. The broken line in the figure means the two phase region. Similar results for Fe-33Ni-H alloy are shown in Figs. 23(a), (b), (c) and Fig. 24.

From the obtained values of heat of dissociation shown in Figs. 19, 22 and 24, we can determine the qualitative relations for the coefficients in eq. (4.2) as follows:

$$\alpha_{Pd} < \alpha_{Ni} < \alpha_{Fe\text{-}Ni}, \quad \beta_{Pd} < \beta_{Ni} < \beta_{Fe\text{-}Ni} \quad \text{and} \quad 2\gamma_{Pd} \simeq (\gamma_{Ni} \simeq \gamma_{Fe\text{-}Ni}). \qquad (4.3)$$

The above relations are interpreted in terms of elastic dipole interactions and electronic metal-hydrogen interactions in the following section.

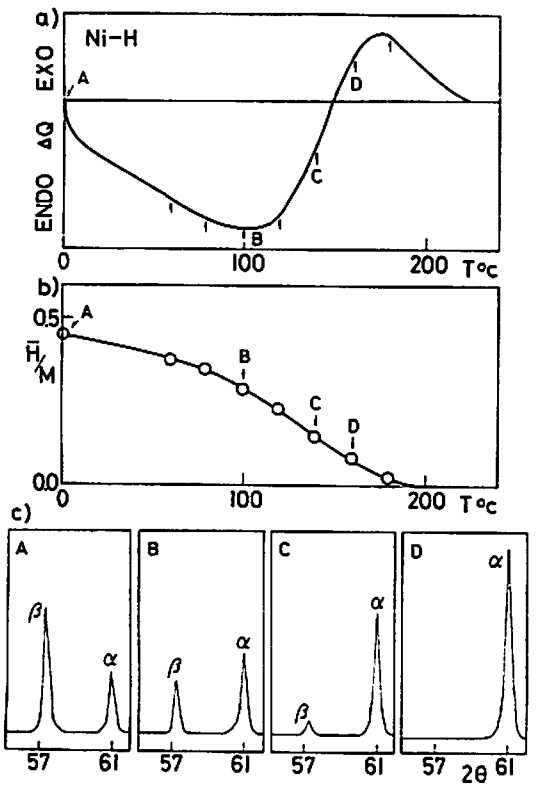

Fig. 21 a) DSC curve of hydrogen outgassing process of Ni-H alloy. The amount 30.2 mg and H/M 0.45. The heating rate 10°C/min. Q=-1.1J. b) Hydrogen concentration at the points by arrows in the figure(a). c) Typical X-ray (200) diffraction profiles. Index from A to D correspond to the same signs in the figures (a) and (b).

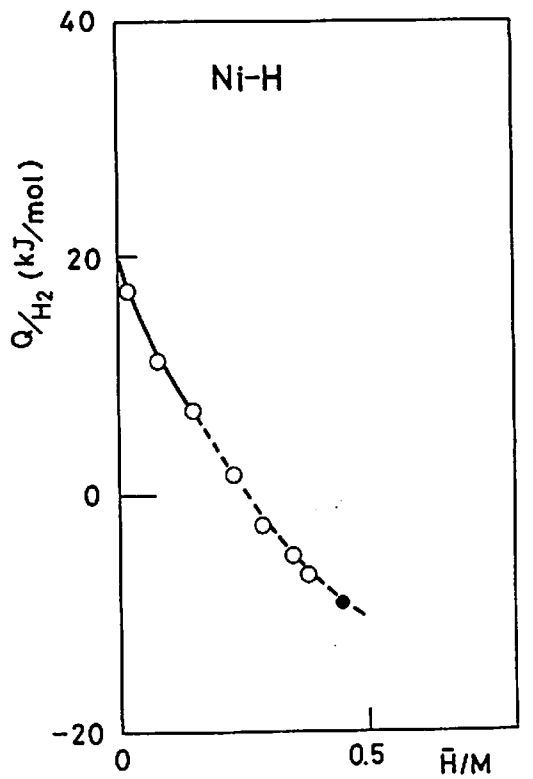

Fig. 22 Heat of dissociation for hydrogen outgassing process of Ni-H alloys as a function of the hydrogen concentration. The broken curve means the two-phase region.

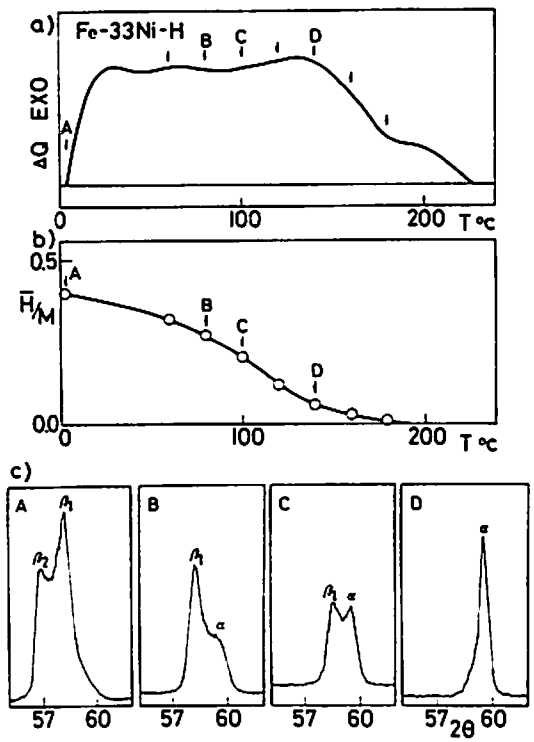

Fig. 23 a) DSC curve of hydrogen outgassing process of Fe-33Ni-H alloy. The amount 41.6mg and H/M 0.40. The heating rate 10 °C/min. Q=+1.9J.
b) Hydrogen concentration at the points by arrows in the figure (a).
c) Typical X-ray (200) diffraction profiles.

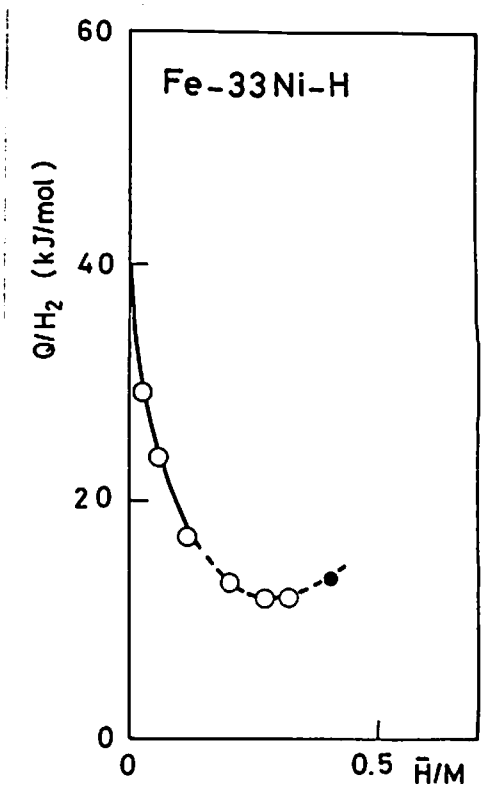

Fig. 24 Heat of dissociation for hydrogen outgassing process of Fe-33Ni-H alloys as a function of the hydrogen concentration. The broken curve means the two-phase region.

§4. Discussion

4.1 Formulation of the total energy of the metal-hydrogen system

A hydrogen atom occupying an octahedral interstitial site in a fcc metal will push aside metal atoms around it and give rise to a long-range strain field. At the same time, local electronic structure is also considerably changed as was mentioned in the last chapter. In this section, the formula-

tion of the total energy of the metal-hydrogen system is done by using the model Hamiltonian which was first proposed by Alefeld,[80] and later by Wagner and Horner[81,82] and Mehlmann et al.,[83] as is given by the following expression:

$$H_{total} = H_{M-M} + H_{H-H} + H_{M-H} \quad . \tag{4.4}$$

The metal-metal interaction, H_{M-M}, is described in a Taylor series by taking account of the elastic energy as

$$H_{M-M} = \Phi_{(R)} + \frac{1}{2} \sum_{m,n} \phi^{mn} v^m v^n \ \ldots, \tag{4.5}$$

where the first order term for v becomes zero because of the force equilibrium condition. The notation v^m means a displacement of the m-th metal atom from the position R^m in the hydrogen-free lattice and ϕ^{mn}'s are force constants. The change of the force constants by hydrogenation may be estimated from a measurement of Young's modulus, for instance. The decrease of the Young's modulus of Pd-H alloy is about 10 % by the absorption of hydrogen as much as H/M=0.7.[87] However, the force constant will be taken as that for hydrogen free lattice and the hydrogen concentration dependence of the force constant will be neglected in the latter semiquantitative evaluation.

The second term H_{H-H} in eq. (4.4) is the electronic interaction between hydrogen atoms, and given by,

$$H_{H-H} = \frac{1}{2} \sum_{a,b} U_{ab} \tau_a \tau_b, \tag{4.6}$$

where τ is the occupation number (τ=1 or 0) in an interstitial site. The interaction U_{ab} may be small, because the distance between nearest hydrogen atoms in the present metals and alloys is about three times longer than that of hydrogen molecule.

For the metal-hydrogen interaction, H_{M-H}, in eq. (4.4), we assume in the first place that the interaction is given by the sum of two-body potentials;

$$H_{M-H} = \sum_{a,n} \Psi(|X^a, Y^m|)\ \tau_a\ , \qquad (4.7)$$

where a distorted interstitial site X^a is expressed by the displacement U^a plus the position Q^a of the a-th interstitial site in hydrogen-free lattice and Y^m is equal to R^m plus V^m. The equation is expanded in powers of the displacements U^a and V^m, that is,

$$H_{M-H} = \sum_{a,m} \Psi(R^m, Q^a)\ \tau_a + \sum_{a,m} \psi^m(R^m, Q^a)\ \tau_a\ V^m \ldots, \qquad (4.8)$$

where the partial derivative of H_{M-H} with respect to U is zero because of the force equilibrium condition on hydrogen atoms and the higher order terms are neglected except for the quadratic term for V^m. The term was reduced and renormalized into the force-constants ϕ^{mn}'s in eq. (4.5), and, therefore, a part of the elastic constants change as was mentioned before may be due to this term. The second term in eq. (4.8) is called the elastic dipole interaction, which means that the a-th hydrogen atom is attracted or repelled by the elastic field induced by a displacement of the m-th metal atom.

The term will be rewritten by using the force constants in the following paragraph and evaluated. The first term in eq.(4.8) corresponds to an important part of the chemical potential of hydrogen atoms, which is a function of the hydrogen concentration. In the case of a transition metal-hydrogen system, the Fermi energy will rise gradually with the increase of hydrogen concentration since the unoccupied high-density states in the d-band will be filled with the transferred electrons, and, then, it will rise steeply because the s-band with the low density of states will be filled after filling up the d-band. The above consideration leads us to the conclusion that the change of the first term behaves in parallel with that of the Fermi energy, gradually increasing in the beginning and rising steeply with the increase of the hydrogen concentration.

Finally, the model Hamiltonian for the metal-hydrogen system was obtained in the following approximated form.

$$H_{total} = \Phi + \frac{1}{2} \sum_{m,n} V^m \phi^{mn} V^n + \sum_a \Psi_{(\bar{\tau})} \tau_a + \sum_{a,m} \psi^{ma} \tau_a V^m \quad . \quad (4.9)$$

The displacements V^m's in the equation are determind from the equilibrium condition $\overline{\partial H_{total} / \partial V^m} = 0$, and, therefore, we can obtain the relation

$$\sum_n \phi^{mn} V^n = - \sum_a \psi^{ma} \tau_a \quad . \quad (4.10)$$

From the relation, we can evaluate the mean value of unknown parameter ψ^{ma} by using the value of force-constants and the

experimental data of the lattice expansion by hydrogenation giving the relation between the mean value of V and τ. In order to calculate the total energy, the second and last elastic terms in eq. (4.9) can be bound and written in the form, $-\frac{1}{2}\sum_{a,b} W_{ab}\tau_a\tau_b$, where W_{ab} is the elastic interaction energy between hydrogen atoms. Therefore, eq. (4.9) is rewritten in the following form.

$$H_{total} = \Phi + \sum_{a} \Psi_{(\bar{\tau})}\ \tau_a - \frac{1}{2}\sum_{a,b} W_{ab}\tau_a\tau_b \ . \qquad (4.11)$$

4.2 Evaluation of the dissociation energy of hydrides

In order to compare the total energy of the system with the experimental values as was given in eq. (4.2), we use the average values, $\bar{\tau}=N_H/N_I \equiv n$ and $\overline{\tau_a\tau_b} = \bar{\tau}_a\delta_{ab} + (1-\delta_{ab})\bar{\tau}_a\bar{\tau}_b$ and from eq. (4.11) we obtain the total energy, H_{total} ;

$$H_{total} = \Phi + \Psi_{(n)}N_H - \frac{1}{2}\left(\frac{N_H}{N_I}\right)\sum_{a} W_{aa} - \frac{1}{2}\left(\frac{N_H}{N_I}\right)^2 \sum_{a\neq b} W_{ab} \ , \qquad (4.12)$$

where N_H and N_I are the number of hydrogen atoms and that of the interstitial sites in a metal. The evaluation of the elastic interaction energy, W, was first proposed and given by Kanzaki[85] for the substitutional defect in solid argon, and later, has been done by Wagner and Horner[81,82] for the fcc metal-hydrogen systems as following expression.

$$\sum_{a} W_{aa} \simeq \frac{N_L N_I}{V C_{11}} P^2 , \tag{4.13}$$

and

$$\sum_{a \neq b} W_{ab} \simeq \frac{K_T N_I^2}{V} P^2 , \tag{4.14}$$

where $P=(1/K_T)(\Delta V/N_H)$ is the force dipole constant. Notations C_{11}, K_T, N_L, V and ΔV are used to denote the elastic constant, compressibility, the number of metals, the volume of the system and the volume change, respectively.

All terms on the right hand side of eq. (4.12) except for the first term Φ, which is the lattice energy of hydrogen-free system as a standard, are equal to the formation energy of the released and isolated hydrogen atoms out of the metallic lattice. The released hydrogen atoms will associate to form molecules on the surface of the specimen. Therefore, the enrgy change in the outgassing process can be evaluated from the formation energy, ΔH_{total}, and the recombination energy of a nascent hydrogen and desorption energy of the hydrogen molecule, E_D. Experimentally, this change is evaluated by using eq. (4.2). Accordingly, from the following equation

$$\frac{H_{exp}}{\text{mol of } H_2} = \frac{2\Delta H_{total} + N_{H_2} |E_D|}{\text{mol of } H_2} , \tag{4.15}$$

we have the relations,

$$\alpha = 2\Psi_{(0)} - \sum_{a} W_{aa} + |E_D| \quad , \tag{4.16}$$

and

$$-\beta n + \gamma n^2 = 2 \frac{\partial \Psi}{\partial n} n + \frac{\partial^2 \Psi}{\partial n^2} n^2 - \sum_{a \neq b} W_{ab} \, n \quad , \tag{4.17}$$

where the second term in eq. (4.12) is expressed by a Taylor series of n.

The coefficients, α's, of Pd-H, Ni-H and Fe-33Ni-H alloys estimated from Figs. (20), (22) and (24) are -15 kJ/mol, +20 kJ/mol and +40kJ/mol, respectively. On the other hand, the values of $\sum_{a} W_{aa}$ in eq. (4.16) are evaluated as about 50 kJ/mol for Pd-H alloy and 61 kJ/mol for Ni-H alloy and E_D is about 436kJ/mol.[13] For the evaluation of the elastic interaction energy, W, per primitive cell unit, the following data are used;

$N_L=1$, $N_I=1$, $V_{Pd}=1.42\times10^{-23}cm^3$, $V_{Ni}=1.11\times10^{-23}cm^3$, $C_{11}^{Pd}=2.27\times10^{12}dyn/cm^2$,[86] $C_{11}^{Ni}=2.50\times10^{12}dyn/cm^2$,[86] $K_T^{Pd}=0.553\times10^{-12}cm^2/dyn$,[86] $K_T^{Pd}=0.538\times10^{-12}cm^2/dyn$[86] and $\Delta V=2.0\times10^{-24}cm^3$ per $0.7N_H$ for palladium and nickel.[87]

Although the detailed theory for the electronic metal-hydrogen interaction energy, $\Psi_{(0)}$, is lacking, we may evaluate it experimentally by substituting the other two values in eq. (4.16), and find that the value of $\Psi_{(0)}$ for Pd-H alloy is smaller than that for Ni-H alloy and that for Fe-33Ni-H alloy will be the largest. This inequality will be discussed on the basis of differences in the d-electrons configuration of the host atoms in the following chapter.

The experimental value on the left hand side and the evaluation on the right in eq. (4.17) for Pd-H and Ni-H alloys are shown in Fig. 25. The elastic dipole energy represented by the 3rd term in the right hand side of eq. (4.17) is given by solid lines by using the values of $\sum_{a \neq b} W_{ab}$, 63 kJ/mol for Pd-H alloy and 82 kJ/mol for Ni-H alloy, which are calculated from eq. (4.14) as mentioned before. Dotted-and-dashed lines mean the change of the electronic metal-hydrogen interaction energy, corresponding to the first and second terms in the right hand side of eq.(4.17). This change was evaluated by using the band filling model as was mentioned in the last chapter, where band calculations for transition metals have been provided by Switendick[88] for instance, and the number of transferred electron which are

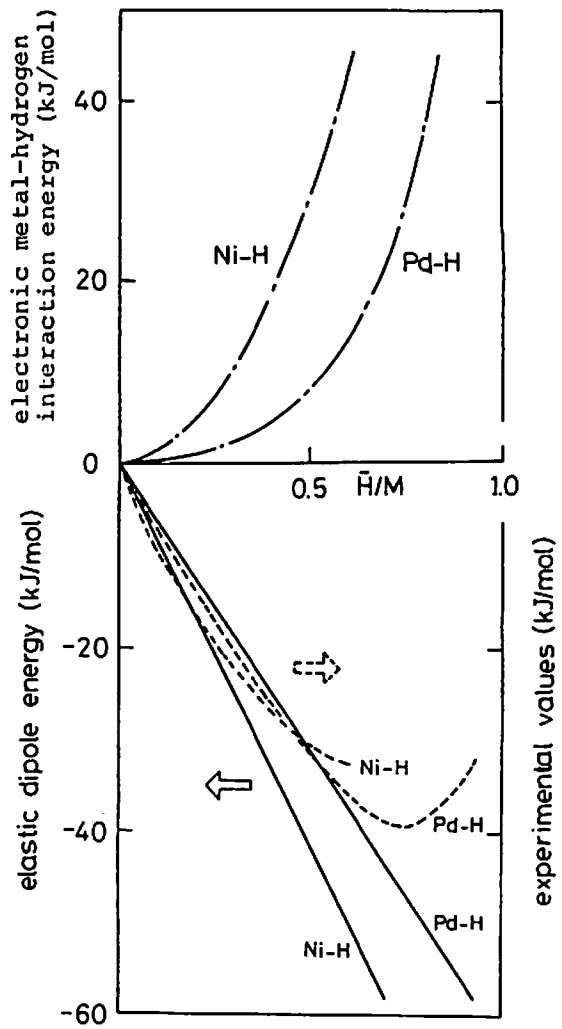

Fig. 25 The evaluation of eq. (4.17) for Pd-H and Ni-H alloys. Solid lines mean the elastic dipole energy represented by the 3rd term in the right hand side of eq. (4.17). Dotted-and-dashed lines show the change of the electronic metal-hydrogen interaction energy corresponding to the 1st and 2nd terms in the right of eq. (4.17). The observed values of the left hand side of eq. (4.17) are shown by dotted lines.

produced by metal-hydrogen interaction can be estimated as a function of hydrogen concentration by using the experimental data of magnetic susceptibility for Pd-H and Ni-H alloys[23,83] and the results of Mössbauer effect of Fe-33Ni-H alloy in Fig. 15.

The observed values of the left hand side of eq. (4.17) are shown by broken lines for Pd-H and Ni-H alloys. The agreement between the calculation and experiment is good. In the figure, the solid line of elastic dipole energy for the Ni-H alloy is steeper than that for the Pd-H alloy, since the elastic properties of matrices are different from each other, that is, $K_T(Ni) < K_T(Pd)$ and $C_{11}(Ni) > C_{11}(Pd)$. The change of the electronic metal-hydrogen interaction energy by hydrogenation for Ni-H alloy is larger than double that for Pd-H alloy. This may arise from that only a half of the unoccupied states of d-band of nickel is filled by the electrons from hydrogen because of the spin polarization of the d-electrons, while, in paramagnetic palladium two spin states in d-band are unoccupied. Fe-33Ni alloy is ferromagnetic and behaves similar to nickel. Therefore, the relation, $2\gamma_{Pd} \simeq (\gamma_{Ni} \simeq \gamma_{Fe-Ni})$, is maintained in eq. (4.2). In conclusion, we can interprete the results of heat of dissociation for Pd-H, Ni-H and Fe-33Ni-H alloys in terms of the energy of elastic dipole interactions and electronic metal-hydrogen interactions, which are the important factor to describe the mechanism of hydride formation. The above interpretation will be also adaptable to copper which has

the same fcc crystal structure and makes extremely unstable hydride.[1,13] The d-band of copper is filled completely in contrast with the above metals and alloys, and, therefore, the change of the Fermi energy of Cu-H alloy may be steeper than that of Pd-H and Ni-H alloys.

Chapter 5. DSC Thermal Analysis and Mössbauer Spectroscopy of Pd-C-H, Ni-C-H and fcc Fe-Ni-C-H Alloys

§1. Introduction

In chapter 2, it was found that the hydride in Pd-C alloy was less stable than in carbon free palladium, while the hydrides in fcc Fe-Ni-C alloys were more stable than in carbon free ones. Such a suppression or enhancement of hydrogen absorption by carbon atoms will not arise from a simple effect. In general, the solubility of carbon in metals is low, but, when dissolved in a metal lattice, the solute atoms give rise to large electronic changes and lattice distortion in their vicinity.

The electronic changes of host atoms around carbon atoms have been studied by means of Mössbauer effect of fcc Fe-Ni-C alloys, and quantitative evaluation of the environmental effect of carbon on the host atoms was done, as well as that of hydrogen atoms, as were mentioned in chapter 3. In the last chapter, it was shown that the DSC measurements of hydrogen outgassing process in the above carbon free alloys were done and the metal-hydrogen bonding energy was evaluated by the energy change of Fermi level and the elastic energy of lattice distortion.

In this chapter, outgassing process of hydrogenated Pd-C, Ni-C and fcc Fe-Ni-C alloys investigated by means of thermal analysis and Mössbauer spectroscopy will be introduced and analyzed. Comparing them with those of carbon free alloys

in the last chapter, the effect of carbon on the stability of hydrogen in metals is discussed by combining the electron theory and lattice distortion theory.

§2. Experimental Results and Analyses

2.1 Procedures

Carburization of the metals and alloys was done in the same condition as mentioned in chapter 2. Hydrogen was supplied by the same procedures as in the last chapter. The thermal analysis, Mössbauer effect, X-ray diffraction and gas volumetric measurements have also been precisely shown in the preceding chapters.

2.2 DSC on Pd-C-H, Ni-C-H and Fe-33Ni-C-H alloy

In the case of the hydrogen outgassing process of the above carburized alloys, the same analysis as for the carbon free alloys in the last chapter was applied. Figure 26(a) shows the DSC curve of Pd-C-H alloy. The residual amount of hydrogen and X-ray profile of specimens are shown in Figs. 26 (b) and (c), respectively. Small arrows in Fig. 26(a) indicate the points of sampling. Figure 27 indicates the heat of dissociation for Pd-C-H alloy obtained through the same treatment as in the case of carbon-free one in the last chapter. Open and full circles in the figure also correspond to the same symbols in chapter 4.3.2. The dotted curve in the figure means the two phase region as was mentioned in the last chapter. The broken curve in the figure represents the heat of dissociation for carbon-free

Pd-H alloy obtained in the last chapter. Comparing the curve for Pd-C-H alloy with that for Pd-H alloy in the figure, qualitative relations for the coefficients in eq. (4.2), $H_{exp}/n=\alpha-\beta n+\gamma n^2$, are obtained as follows:

$$\alpha_{Pd\text{-}C\text{-}H} > \alpha_{Pd\text{-}H},\ \beta_{Pd\text{-}C\text{-}H} > \beta_{Pd\text{-}H} \text{ and } \gamma_{Pd\text{-}C\text{-}H} \simeq \gamma_{Pd\text{-}H} \cdot \qquad (5.1)$$

As recognized by overlapping the DSC curve for Pd-C-H alloy

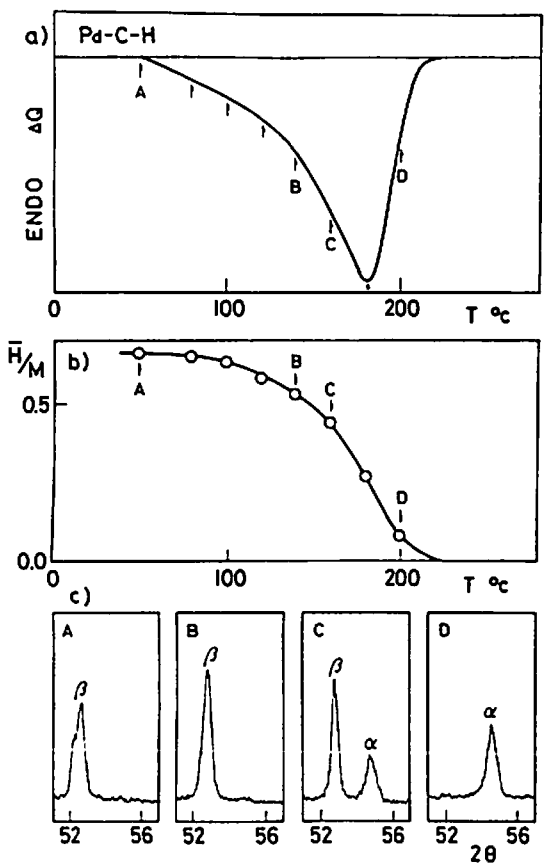

Fig. 26 a) DSC curve of hydrogen outgassing process of Pd-C-H. The amount 20.6mg and H/M 0.66. The heating rate 10°C/min. Q=-4.0J.
b) Hydrogen concentration at the points by arrows in the figure (a).
c) Typical X-ray (200) diffraction profiles.

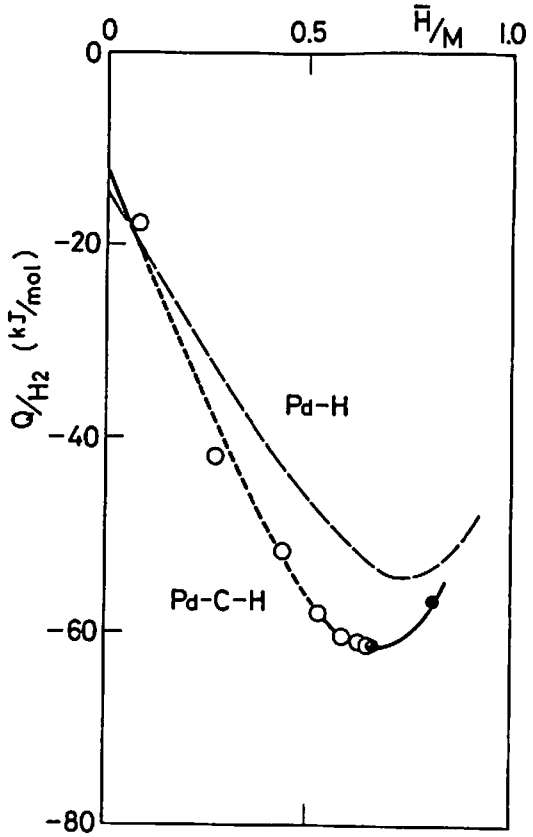

Fig. 27 Heat of dissociation for hydrogen outgassing process of Pd-C-H alloys as a function of the hydrogen concentration. The dotted curve means the two-phase region. The broken line is that of Pd-H alloy in Fig. 20.

in Fig. 26(a) on the curve of carbon-free one in Fig. 19(a), the temperature of endothermic peak deviates to the low temperature side by about 20 degrees by carburization. This change of the dissociation temperature corresponds to the inequality of the coefficient, α, in eq. (5.1) as was discussed in the last chapter.

Similar results for Ni-C-H and Fe-33Ni-C-H alloy are obtained and shown in Figs. 28(a),(b), (c) and Fig. 29 for Ni-C-H alloy and in Figs. 30(a), (b), (c) and Fig. 31 for

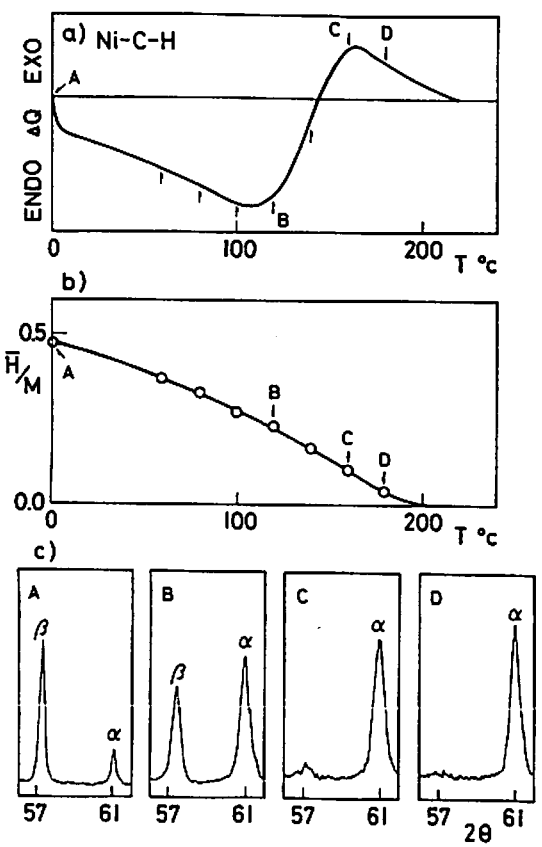

Fig. 28 a) DSC curve of hydrogen outgassing process of Ni-C-H alloy. The amount 36.7mg and H/M 0.47. The heating rate is 10°C/min. Q=-1.4J. b) Hydrogen concentration at the points by arrows in the figure (a). c) Typical X-ray (200) diffraction profiles.

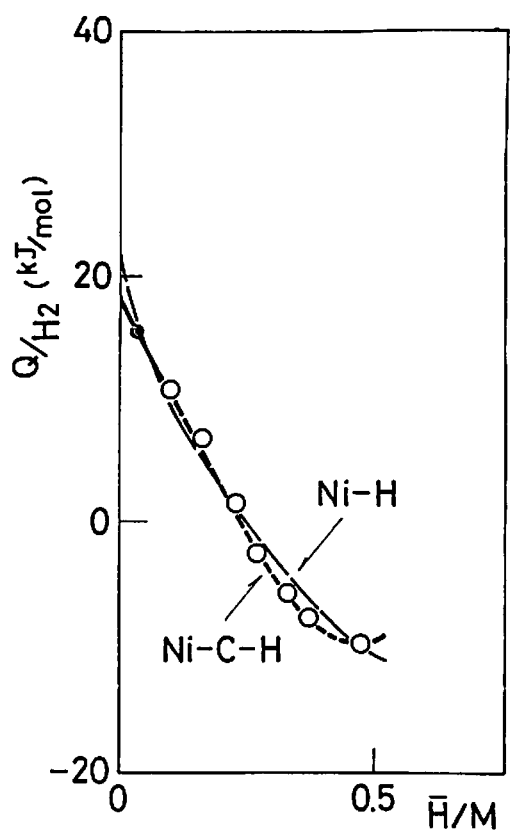

Fig. 29 Heat of dissociation for hydrogen outgassing process of Ni-C-H alloys as a function of hydrogen concentration. The dotted curve means the two-phase region. The broken line is that of Ni-H alloy in Fig. 22.

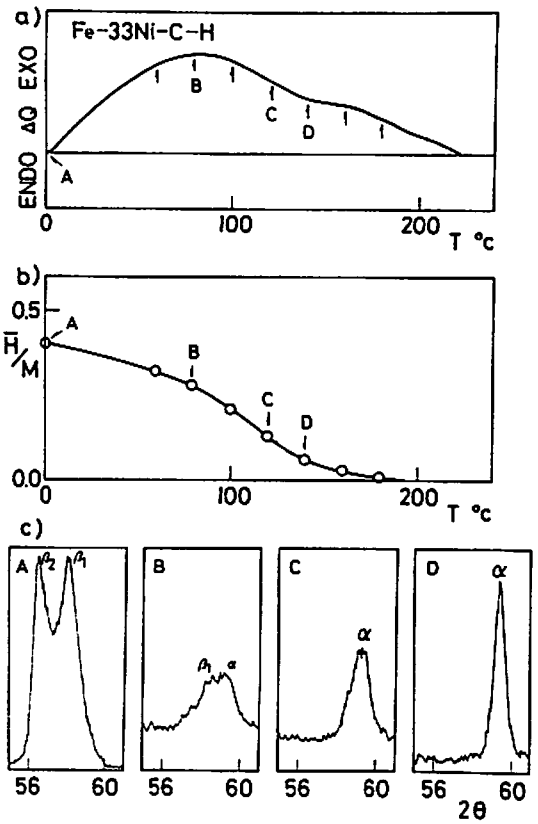

Fig. 30 a) DSC curve of hydrogen outgassing process of Fe-33Ni-C-H alloy. The amount 33.5mg and H/M 0.40. The heating rate 10°C/min. Q=+1.1J.
b) Hydrogen concentration at the points by arrows in the figure (a).
c) Typical X-ray diffraction profiles.

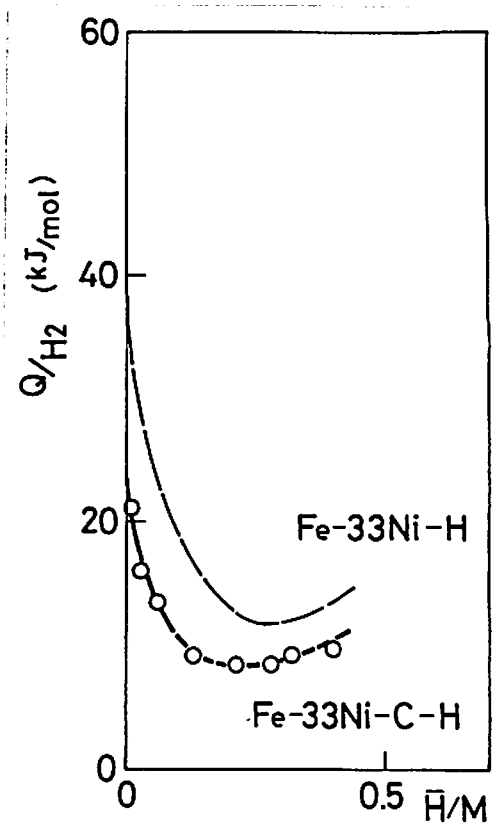

Fig. 31 Heat of dissociation for hydrogen outgassing process of Fe-33Ni-C-H alloys as a function of the hydrogen concentration. The dotted curve means the two-phase region. The broken line is that of Fe-33Ni-H alloy in Fig.24.

Fe-33Ni-C-H alloy, and the curves of dissociation energy for carbon-free ones are shown by the dotted lines in Figs. 29 and 31. Their coefficients' relations in eq. (4.2) are

$$\alpha_{Ni\text{-}C\text{-}H} \lesssim \alpha_{Ni\text{-}H}\ , \qquad \beta_{Ni\text{-}C\text{-}H} \gtrsim \beta_{Ni\text{-}H} \qquad \text{and } \gamma_{Ni\text{-}C\text{-}H} \simeq \gamma_{Ni\text{-}H}\ , \tag{5.2}$$

and

$$\alpha_{Fe\text{-}Ni\text{-}C\text{-}H} < \alpha_{Fe\text{-}Ni\text{-}H}\ , \ \beta_{Fe\text{-}Ni\text{-}C\text{-}H} > \beta_{Fe\text{-}Ni\text{-}H} \quad \text{and } \gamma_{Fe\text{-}Ni\text{-}C\text{-}H} \simeq \gamma_{Fe\text{-}Ni\text{-}H}\ . \tag{5.3}$$

The values of α's become small when nickel and Fe-33Ni alloy are carburized, which corresponds to the slightly higher dissociation temperature of carburized alloys than that of carbon-free ones as shown in Fig. 21(a) and 28(a) and in Figs. 23(a) and 30(a), respectively. The inequality relations in eqs. (5.1), (5.2) and (5.3) will be discussed later on the basis of the lattice distortion theory and electron theory.

2.3 Mössbauer spectroscopy of Fe-33Ni-C-H alloy

For the investigation of the local electronic structure around the interstitial hydrogen and carbon atoms, Mössbauer spectroscopy is powerful as was shown in a previous chapter. By carburization of Fe-33Ni alloy to the carbon concentration of about 1.5 at.%, the Mössbauer spectrum changed from the broken lines in Fig. 32(a) to the broken lines in Fig. 32(b), exhibiting some additional shoulders, which arose from the iron atoms first neighbouring with carbon atoms. This first neighbour component is indicated by the small peaks drawn by dot-and-dashed line in the figure (b). The two-dot-dashed line in the figure also shows the component of the second and third neighbour irons, and, the remainder of the spectrum is due to the components of further neighbours and totally unaffected iron atoms as was analyzed in chapter 3.

The Mössbauer spectra of hydrogenated Fe-33Ni and Fe-33Ni-C alloys are shown by the experimental points in Figs. 32(a) and (b), where the hydrogen concentrations in atom ratio are

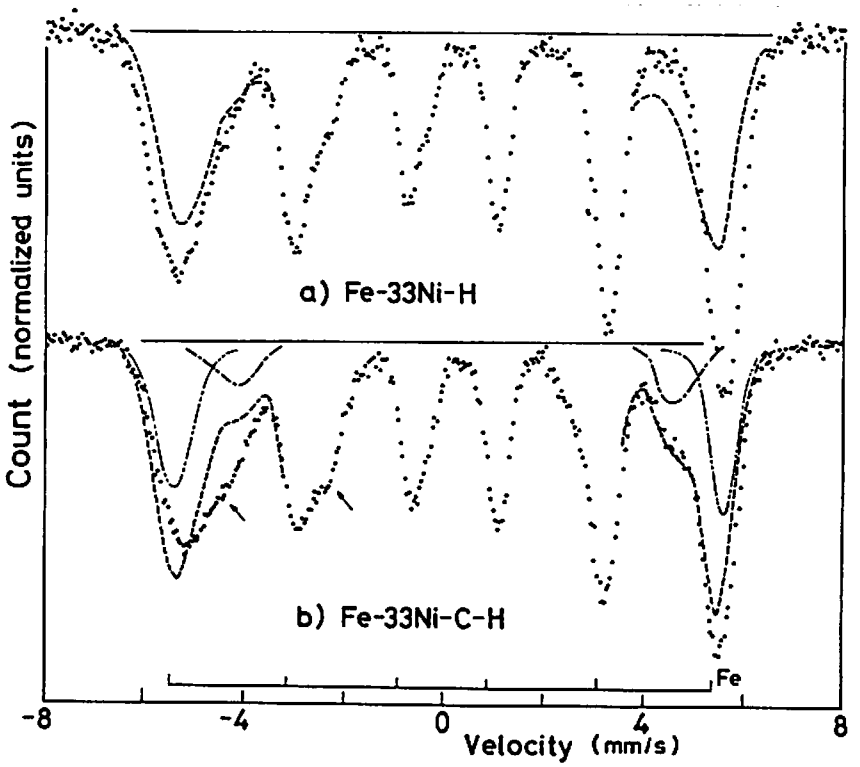

Fig. 32 Mössbauer spectra of Fe-33Ni alloys at 77K.
a) Hydrogenated Fe-33Ni alloy.
The broken line indicates the spectrum of hydrogen free Fe-33Ni alloy.
b) Hydrogenated Fe-33Ni-C alloy.
The broken line indicates the spectrum of hydrogen free Fe-33Ni-C alloy. The dot-and-dashed line means the component affected by the first neighbour interstitial octahedral site carbon. The two-dot-dashed line means the component affected by the second and third neighbour interstitial octahedral site carbon.

H/M=0.30 and 0.31, respectively. As was mentioned in the chapter 3, the characteristic weak ferromagnetic components of the Invar alloy corresponding to a wide spread dip from the base line of the central part of the spectrum rapidly disappeared by addition of a small amount of interstitial

elements and turned to the strong ferromagnetic ones. The changes of the ferromagnetic components by hydrogenation of Fe-33Ni-C alloy is summarized in Fig. 33, in which the hydrogen concentration dependence of the internal magnetic field and of the isomer shift were determined simply from the peak position of the ferromagnetic six line main spectra, where typical Mössbauer spectra are shown in Figs. 34(a) to (h). The internal field shown Fig. 33 linearly increases with the hydrogen concentration until 3 at.% hydrogen and the linearly decreases, exhibiting a maximum like the Slater-Pauling curve. The change of the isomer shift is in proportion to the hydrogen concentration below 10at.%. These curves of internal field and isomer shift fit well those of the carbon-free ones in Fig. 15, respectively, except for the parallel shift along the horizontal line due to the effect of carbon atoms.

In addition to the above overall significance of the

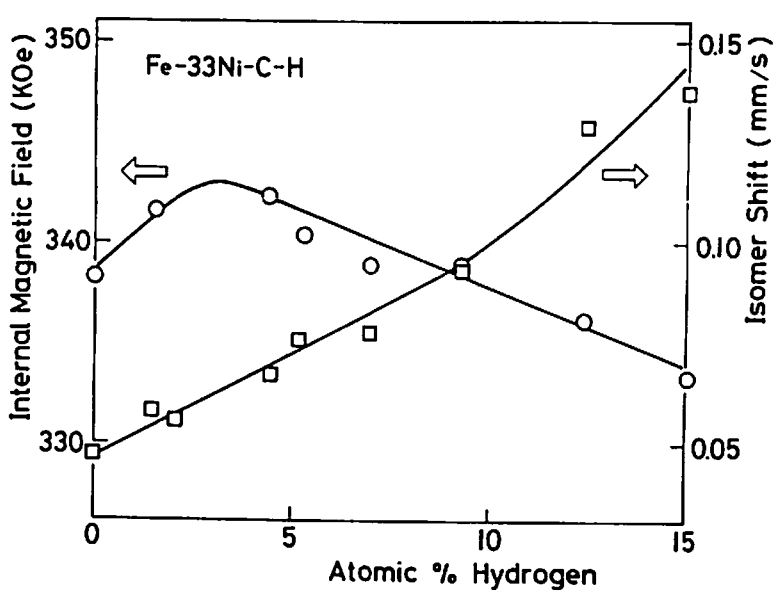

Fig. 33 The values of the internal magnetic field and the isomer shift of Fe-33Ni-C-H alloys against the hydrogen concentration.

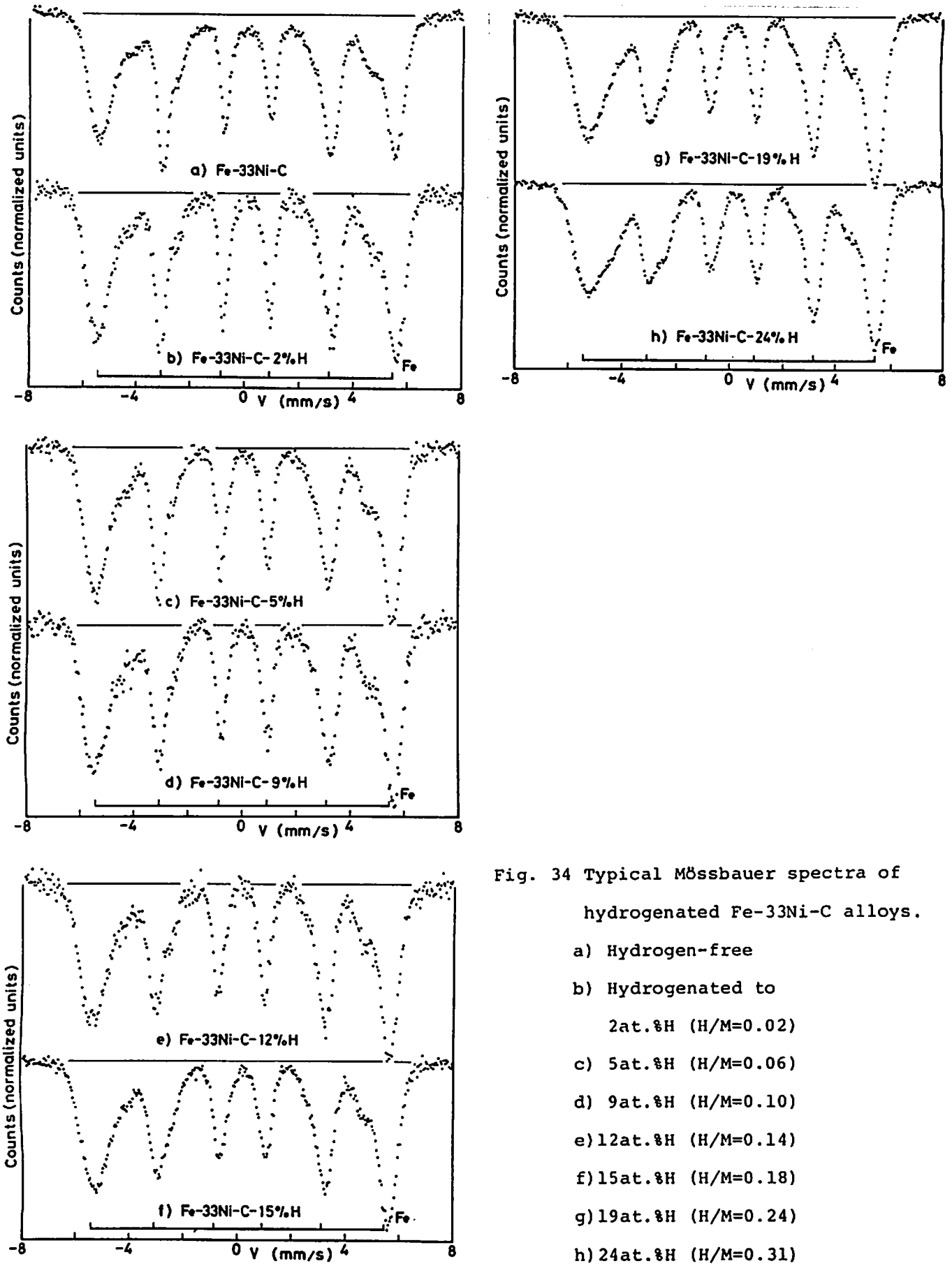

Fig. 34 Typical Mössbauer spectra of hydrogenated Fe-33Ni-C alloys.

a) Hydrogen-free

b) Hydrogenated to 2at.%H (H/M=0.02)

c) 5at.%H (H/M=0.06)

d) 9at.%H (H/M=0.10)

e) 12at.%H (H/M=0.14)

f) 15at.%H (H/M=0.18)

g) 19at.%H (H/M=0.24)

h) 24at.%H (H/M=0.31)

spectral changes by hydrogenation, individual changes of each spectral component appearing in Fig. 32 enabled us to find the local influences and configurations of hydrogen atoms around the iron atoms neighbouring and unneighbouring with carbon atoms. For instance, considerably large swelling took place on the inner side of the first and second leftest peaks by hydrogenation of carburized specimen, as indicated by two small arrows in the figure (b), which did not appear in the carbon-free specimen as in the figure (a). By subtracting the hydrogen unaffected components from the whole spectrum of the hydrogenated alloy in Figs. 32(a) and (b), respectively, it was possible to separate the spectrum into the hydrogen-affected and unaffected parts. The analysis showed that the swelled part correspond to the second and third neighbours, which were largely shifted by hydrogenation. On the other hand, the first neighbour components, drawn by the dot-and dashed lines in the figure (b), were scarcely shifted by hydrogenation up to the concentration of H/M=0.3. This means that the iron atoms first-neighbouring with carbon atoms did not attract hydrogen atoms while the hydrogen concentration was enhanced around the second and third neighbours, giving rise to the large shifts of the latter's spectral components. Taking account of the internal field change versus hydrogen concentration curve in Fig. 33, the hydrogen concentration around the second and third neighbour irons was roughly estimated as about 0.4. This effect of carbon on the hydrogen concentration around iron atoms will be discussed in the following section.

§3. Discussion

3.1 Formulation of the total energy of the metal-hydrogen-carbon system

In the last chapter, we obtained the formulation of the total energy of the metal-hydrogen system by using the elastic lattice distortion energy and electronic metal-hydrogen interaction energy, as expressed by eq. (4.11). The solubility of carbon in the metals and alloys in the problem is as low as 1.5 at.% to 2.0 at.%.[23,60,61] While, the Goldsmith radius of interstitial carbon is fairly large, giving rise to the large lattice distortion and electronic changes spread around the carbon atom, which will also change the dissociation energy of hydride in the carburized metals.

In order to evaluate the dissociation energy of hydride in a carburized metal, an expansion of the model Hamiltonian as was given in eq. (4.4) will be made, and eq. (4.9) in the last chapter will be rewritten as the following approximated form,

$$H^{c}_{total} = \phi^{c} + \frac{1}{2}\sum_{m,n} V^{m}\phi^{mn c}V^{n} + \sum_{a} \Psi_{(n,n^{c})}\tau_{a} + \sum_{a,m} \psi^{ma}\tau_{a}V^{m} + X_{C-H} \quad , \quad (5.4)$$

where index c means the carburized system. In the equation, the electronic carbon-hydrogen interaction, U_{C-H}, is neglected as well as U_{H-H} in eq. (4.6). With respect to the force constants in the second term, their changes by carburization are considered. The chemical potential of hydrogen atoms in the third term in eq. (5.4) will depend on the concentration of

carbon too, since the infused carbon also raise the Fermi level of the system. The elastic carbon-hydrogen interaction, X_{C-H}, of the last term is brought about by lattice distortion around carbon atoms, and can be evaluated in analogy with that of hydrogen as was mentioned in chapter 4.4.1.

$$X_{C-H} \simeq -\frac{1}{2} \sum_a \omega_{ac} n^c \tau_a \quad , \tag{5.5}$$

where

$$\omega_{ac} \simeq \frac{K_T^c N_I^2}{V} (P^c)^2, \qquad P^c = \left(\frac{1}{K_T^c}\right)\left(\frac{\Delta V^c}{N_c}\right) \tag{5.6}$$

and N_c is the number of carbon atom. By using the equilibrium condition, $\overline{\partial H^c_{total}/\partial V^m} = 0$, we can obtain the following formuration;

$$H^c_{total} = \phi^c + \sum_a \Psi(n, n^c)\tau_a - \frac{1}{2}\sum_{ab} W_{ab}\tau_a\tau_b - \frac{1}{2}\sum_a \omega_{ac} n^c \tau_a \ . \tag{5.7}$$

Finally, the dissociation energy in the outgassing process can be evaluated theoretically by using eq. (5.7) and can be bound with the experimental equation (4.2) through the same manner as in the case of metal-hydrogen system, and the following relations of coefficients are obtained.

$$\alpha^c = 2\Psi(0, n^c) - \sum_a W^c_{aa} - \omega_{ac} n^c + |E_D| \quad , \tag{5.8}$$

and

$$-\beta^c n + \gamma^c n^2 = 2\frac{\partial \Psi(0, n^c)}{\partial n} n + \frac{\partial^2 \Psi(0, n^c)}{\partial n^2} n^2 - \sum_{a \neq b} W^c_{ab} n. \tag{5.9}$$

3.2 The effect of carbon on the stability of hydrides

The values of α^C, β^C and γ^C in the left hand side of eqs. (5.8) and (5.9) were given experimentally in the last section, and compared with those of corresponding carbon free systems, the qualitative relations for the coefficients were obtained as shown in eqs. (5.1), (5.2) and (5.3). Since the experimental coefficient of γ^C is approximately equal to γ in all cases, the terms of the electronic metal-hydrogen interaction energy in the right hand side of eqs. (4.17) and (5.9) are equal to each other as follows; $\partial^2\Psi_{(0,n^C)}/\partial n^2 \simeq \partial^2\Psi_{(0)}/\partial n^2$. This relation suggests that the shape of d-band holes of matrix atoms is little changed by carburization, which has been recognized by a preliminary experiment by ESCA and band calculations.[43,88] The coefficient β^C is slightly larger than β in all systems. The difference is represented by using eqs. (4.17) and (5.9) as

$$\beta^C - \beta = -2\left(\frac{\partial\Psi_{(0,n^C)}}{\partial n} - \frac{\partial\Psi_{(0)}}{\partial n}\right) + \left(\sum_{a\neq b} W^C_{ab} - \sum_{a\neq b} W_{ab}\right) . \quad (5.10)$$

Since we can expect the relation, $\partial\Psi_{(0,n^C)}/\partial n \approx \partial\Psi(0)/\partial n$, due to the rigid d-band hole as was discussed in the above, the difference must be due to the larger elastic interaction energy of carburized system than that of carbon-free one. The force constant of a carburized alloy must be larger than that of a carbon-free alloy. The inequality relation between α^C and α is not unique among the alloy systems as follows:

$\alpha^{c}_{Pd-C-H} > \alpha_{Pd-H}$, $\alpha^{c}_{Ni-C-H} \leq \alpha_{Ni-H}$ and $\alpha^{c}_{Fe-Ni-C-H} < \alpha_{Fe-Ni-H}$.

From eqs. (4.17) and (5.9), we can obtain the following equation.

$$\alpha^{c} - \alpha = 2(\Psi_{(0,n^{c})} - \Psi_{(0)}) - (\sum_{a} W^{c}_{aa} - \sum_{a} W_{aa}) - \omega_{ac} n^{c} . \quad (5.11)$$

The last term in the right hand side of the equation can be estimated for Pd-C and Ni-C alloys by using eq. (5.5), and the values, $\omega_{ac} n^{c}$, are 5 and 6.7 kJ/mol, respectively, where the data of elastic constants were used as the values of carbon-free metals and ΔV^{c} per primitive cell is $1.0 \times 10^{-25} cm^{3}$ per 0.015 carbon atoms[23]. The value in the second parenthesis in the right hand side of the equation will be roughly estimated by combining the eqs. (4.13), (4.14) and (5.10) as about 1 kJ/mol for both palladium and nickel alloys with the assumption that the force constant increases by 1% by carburization by 1.5% carbon. Likewise, the values of the last two terms in eq. (5.11) for Fe-Ni alloy must be approximately equal to those for nickel, as was discussed in the last chapter. On the other hand, the experimental value of the left hand side in eq. (5.10) is +2kJ/mol for palladium, -4kJ/mol for nickel and -17kJ/mol for Fe-Ni alloys. Therefore, the change of the electronic metal-hydrogen interaction energy by carburization, i.e., the value of the first term in the right of the equation, is roughly +8kJ/mol, +2kJ/mol and -9kJ/mol for palladium, nickel and Fe-Ni alloys, respectively.

One origin of the electronic changes by carburization is the increase of the Fermi level as was discussed in chapter 3, which can be detected from the shift of the minimum point to the low concentration side in the experimental curves in Figs. 27, 29 and 31. Because, the point indicates the filling up of d-holes by hydrogenation as was discussed in the last chapter. The mean value of the change by carburization can be roughly estimated from the experimental values of magnetic susceptibility[23] to be 2kJ/mol for palladium alloy and 4kJ/mol for nickel and Fe-Ni alloys. Actually, the local electronic change around a carbon atom may be larger than the above mean values as was shown in the interpretation of the Mössbauer data in chapter 3. Nevertheless, this effect of the increase of the Fermi level by carburization can not explain even qualitatively, because the change of the Fermi level by carburization must be always positive while the experimental values are either positive or negative. Therefore, another effect must be further introduced in the explanation of the change of the electronic metal-hydrogen interaction energy by carburization.

The detailed Mössbauer analysis for Fe-33Ni-C-H alloy in the last section showed that the hydrogen concentration in the very vicinity of the iron atoms which were located at the second and third nearest neighbour positions with carbon atoms was remarkably larger than that in the vicinity of carbon-unaffected iron atoms while that around the carbon-first neighbour iron atoms was very low. On the other hand, the

hydrogen concentration in palladium was reduced by half when the metal was carburized, as mentioned before. The above differences can not be attributed to a simple effect such as of lattice distortion but the electronic effect, i.e., the change of the chemical potential. Although a detailed theory for the electronic metal-hydrogen interaction energy, $\Psi_{(0)}$, in eqs.(4.16) and (5.11) is lacking, the experimental results seem to suggest that the correlations between the orientations and positions of metal , carbon and hydrogen strongly affect the interaction energies between the constituent atoms.

The d-orbital configurations of palladium are different from those of nickel and iron. Their magnetic properties indicate that the electrons in d-shell of nickel and iron in magnetic state tend to occupy the e-orbitals which stretch to the direction toward the first neighbour interstitial site, while the electrons of palladium in non-magnetic state mainly occupy the t-orbitals which extend toward the first neighbour matrix atoms indicating strong itinerancy. Such tendencies of d-configurations is recognized by the molecular orbital calculation.[89] The above mentioned differences of electronic metal-hydrogen interaction energy in different alloys and different neighbouring sites could be explained in terms of these orbital configurations. For instance, a first neighbour interstitial carbon has to face to the e-orbitals of the surrounding matrix metal atoms, and will partially offer its

electrons to them as was mentioned in chapter 3. This e-orbital filling by carbon's electrons would make the occupancy of other first neighbour interstitial site by hydrogen atom difficult since the hydrogen will have to face to the more filled e-orbitals. On the other hand, the second and third nearest carbon will face to t-orbitals, possibly attracting electrons from them through a strong coupling. In the case of nickel or iron, such redistribution of electrons would make holes in the e-orbitals, and could offer an easier environmental condition to hydrogen coming to the second neighbour site. Accordingly, the large effect of hydrogen on the second and third neighbour components and the least effect on the first neighbour component in the Mössbauer spectrum. In the case of palladium, carbon tend to hinder the hydride formation. This is probably because its t-orbitals are mainly filled from the beginning and the second and third nearest carbon would not attract electrons from e-orbitals. Such an interpretation of the differences in chemical potentials by the differences in d-orbital configurations is only tentative and must be subjected further theoretical considerations.

In conclusion, the effect of carbon on the stability of hydrogen in metals is at least qualitatively interpreted in terms of the lattice distortion theory and electron theory.

Conclusions

In the present study, hydrogenated palladium, nickel and fcc Fe-Ni alloys with and without carbon are measured by the ^{57}Fe Mössbauer effect and thermal analysis, and following conclusions were obtained.

1) When the fcc Fe-Ni Invar alloy was carburized, the characteristic weak ferromagnetic part in the Mössbauer spectra disappeared, and, at the same time, a new component with an internal field considerably smaller than that of the main component appeared. The former behaviour is compared with a similar effect by hydrogen. The new component arises from the iron atoms first-neighbouring with carbon atoms. The behaiviour of the internal field of the hydrogenated alloy exhibits a maximum like a Slater-Pauling curve with increasing hydrogen concentration. These changes of the internal field were interpreted on the basis of the electron theory. The environmental effect of interstitial hydrogen and carbon atoms on electronic structures of metal atoms was quantitatively evaluated.

2) The heat of dissociation of hydrogen outgassing process of Pd-H, Ni-H and fcc Fe-Ni-H alloys was obtained as a function of hydrogen concentration. The dissociation energy decreased with the increase of hydrogen concentration, and in a high hydrogen concentration region, it had a minimum value, and, then, increased. To interpret the dissociation energy obtained

by the experiment, the energy change of the whole metal-hydrogen system was evaluated in terms of the elastic lattice distortion energy and the energy of electronic metal-hydrogen interaction. The decrease of the dissociation energy with the increase of hydrogen concentration is mainly due to the elastic relaxation energy of hydrogen atoms in lattice distortion fields of metal atoms. The increase of the dissociation energy in a high hydrogen concentration region is caused by the increase of the Fermi level induced by the electronic metal-hydrogen interaction. From the above results, the mechanism of hydride formation was discussed.

3) The amount of absorbed hydrogen in a fcc carburized Fe-Ni alloy was larger and its hydride was more stable than in carbon-free alloy, while the amount of hydrogen decreased and the hydride was less stable when the palladium was carburized. To investigate the effect of carbon on hydrogen absorption and the stability of hydrogen in metals, outgassing process of carburized and hydrogenated palladium, nickel and fcc Fe-Ni alloys was measured by thermal analysis and Mössbauer effect. The above effect of carbon was interpreted by extending the lattice distortion theory and electron theory mentioned in the above.

Acknowledgements

The author would like to express his hearty thanks to Prof. F. E. Fujita for continuous guidance, stimulative discussions and encouragements throughout the course of this study and also to Prof. H. Suga and Dr. T. Sohmura for their valuable discussions and encouragements. The DSC measurement was performed by using the apparatus in Prof. Suga's laboratory. He wishes to express his thanks to Prof. M. Hirata for valuable coments. He gratefully acknowledges Profs. S. Tamaki, M. Goda, T. Kaga and K. Hoshino of Niigata University for their kind encouragements. Thanks are also due to Mr. T. Hamada for his assistance in the experiments and to Mrs. K. Aizawa and Mr. M. Nakajima of Niigata University for their great help in the preparation of the paper.

References

1) W. M. Mueller: Metal Hydrides, (Academic Press, New York 1968).

2) ed. G. Alefeld and J, Völkl: Topics in Applied Physics, vol.28 and 29 "Hydrogen in Metals vol. 1 and 2" (Springer-Verlag, 1978).

3) K. Nakamura and Y. Sasaki: Zairyō Kagaku 15(1978)110, in Japanese.

4) M. Kitada and G. Kamoshita: Kinzoku zairyō 15(1975)77, in Japanese.

5) Y. Iijima and K. Hirano: Nippon Kinzoku Gakkai Hoh, 14(1975) 599, in Japanese.

6) P. Cotterill: Progress Material Science, vol. 9(Pergamon Press, London, 1961).

7) ed. Nippon Kinzoku Gakkai: Kinzoku to Suiso (Nippon Kinzoku Gakkai, Japan, 1974), in Japanese.

8) M. M. Antonova: Svoistva Gidridov Metallov, (Naukova Dumka, Kiev, SSSR 1975), Translated into Japanese "Kinzokusuisokabutsu no seishitsubinran" (Nisso-Tsushinsha, 1976).

9) V. A. Somenkov: Ber. Bunsenges. Phys. Chem. 76(1972) 733.

10) J. Völkl and G. Alefeld: in Hydrogen in Metals vol. 1 (Springer-Verlag, 1978), ed. G. Alefeld and J. Völkl.

11) E. G. Maksimov and O. A. Pankratov: Sov. Phys. Usp.18 (1976) 481.

12) ed. Japan Institute of Metals: in Hydrogen in Metals "Proceeding of JIMIS-2, Supple. to Trans. JIM 21 (1980)" (Japan Institute of Metals, Japan, 1980).

13) T. R. P. Gibb, Jr.: Progress in Inorganic Chemistry ed. F. A. Cotton vol. 3 (Insci. Wiley, 1962).

14) H. Peisl: in Hydrogen in Metals vol. 1 (Springer-Verlag, 1978), ed. G. Alefeld and J. Völkl.

15) T. Sohmura and F. E. Fujita: J. Magn. & Magn. Mater. 10 (1979) 255.

16) T. Moriya, H. Ino, F.E.Fujita and Y. Maeda: J. Phys. Soc. Jap. 24 (1968) 60.

17) C. Siga, F. E. Fujita and M. Kimura: J. Jpn. Inst. Met. 39 (1975) 1205, in Japanese.

18) E. O. Wollan: Phys. Rev. 122 (1961) 1710.

19) S. Harada, T. Sohmura and F. E. Fujita: Trans. JIM 21 (1980) 281, Supple., "Proceedings JIMIS-2 Hydrogen in Metals, 1979".

20) S. Harada, T. Sohmura and F. E. Fujita: J. Phys. Soc. Jpn. 50 (1981) 2909.

21) S. Harada: J. Phys. F 13(1983) to be published.

22) S. Harada, T. Sohmura and F. E. Fujita: J. Phys. F 13(1983) to be Published.

23) M. C. Cadeville and C. Lerner: Phils. Mag. 33 (1976) 801.

24) ed. Nippon Kinzoku Gakkai: Kinzoku Data Book (Marzen, Japan, 1974).

25) K. Yamakawa: J. Phys. Soc. Japan 47(1979)114.

26) M. Tada and F. E. Fujita: Trans. JIM 21(1980)169, Supple., "Proceedings JIMIS-2 Hydrogen in Metals, 1979".

27) G. Wortmann: J. Phys. (Paris) 37 (1976) c6-333.

28) F. E. Wagner and G. Wortmann: in Hydrogen in metals Vol. 1 (Springer-Verlag,1978), ed. G. Alefeld and J. Völkl.

29) D. E. Eastman, J. K. Cashion and A. C. Switendick: Phys. Rev. Lett. 27 (1971) 35.

30) K. Tanaka, C. Sugiura, S. Nakai and Y. Ohno: Jpn. J. Appl. Phys. 20 (1981) 41.

31) R. M. Cotts: in Hydrogen in Metals Vol. 1 (Springer-Verlag, 1978), ed. G. Alefeld and J. Völkl.

32) N. S. Ho and F. D. Manchester: J. Chem. Phys. 51 (1969) 5437.

33) T. Sohmura and F. E. Fujita: J. Phys. F 8 (1978) 2061.

34) T. Sohmura, F. E. Fujita and M. Okuhata: J. Phys. (Paris) 40 (1979) c2-207.

35) T. Sohmura and F. E. Fujita: J. Phys. F 10 (1980) 743.

36) J. S. Carlow and R. E. Meads: J. Phys. C 2 (1969) 2120.

37) A. E. Jech and C. R. Abeledo: J. Phys. Chem. Solids 28 (1967) 1317.

38) G. K. Wertheim and D. N. E. Buchanan: J. Phys. Chem. Solids 28 (1967) 225.

39) T. Mizutani, T. Shinjo and T. Takada: J. Phys. Soc. Jpn. 41 (1976) 794.

40) M. Ableiter and U. Gonser: Z. Metallk. 66(1975)86.

41) L. J. Swartzendruber, L. H. Bennett and R. E. Watson: J. Phys. F. 6 (1976) L331.

42) H. Adachi, S. Imoto, T. Tanabe and M. Tsukada: J. Phys. Soc. Jpn. 44 (1978) 1039.

43) H. Adachi and S. Imoto: J. Phys. Soc. Jpn. 46 (1979) 1194.

44) S. Kazama and Y. Fukai: J. Phys. Soc. Jpn. 42 (1977) 119.

45) B. Window: J. Appl. Phys. 44 (1973) 2853.

46) ed. A. J. Freeman and M. Shimizu: The Invar Problem (North-Holland, Amsterdam 1979).

47) Y. Nakamura, M. Shiga and N. Shikazono: J. Phys. Soc. Jpn. 19 (1964) 1177.

48) S. Tomiyoshi, H. Yamamoto and H. Watanabe: J. Phys. Soc. Jpn. 30 (1971) 1605.

49) U. Gonser, S. Nasu, W. Keune and O. Weis: Solid State Commun. 17 (1975) 233.

50) F. E. Fujita, C. Shiga, T. Moriya and H. Ino: J. Jpn. Inst. Met. 38 (1974) 1031, in Japanese.

51) C. Shiga, M. Kimura and F. E. Fujita: J. Jpn. Inst. Met. 38 (1974) 1073, in Japanese.

52) H. Adachi and S. Imoto: Nippon Kinzoku Gakkai Hoh: 17 (1978) 490, in Japanese.

53) ed. R. Hashiguchi: Kinzoku Butsurigaku (Asakura, Japan, 1970), in Japanese.

54) R. A. Swalin: Thermodynamics of Solids (Wiley, New york, 1972).

55) A. Sawamoto, N. Takeuchi, A. Hayashi and N. Ohtani: Nippon Kinzoku Gakkai Kōengaiyō (April, 1978).

56) E. O. Wollan, J. W. Cable and W. C. Koehler: J. Phys. Chem. Solids 24 (1963) 1141.

57) ed. Nippon Tetsukō Kyokai: Hagane no Netsushori (Marzen, Tokyo, 1969), in Japanese.

58) S. Miyata: Ph. D. Thesis, Osaka University, (1974).

59) M. C. Cadeville, R. Caudron, P. Costa and C. Lerner: J. Phys. F 4 (1974) L87.

60) ed. M. Hansen and K. Anderko: Constitution of Binary Alloys (Mcgraw-Hill, New Yoyrk, 1958).

61) T. Kase: The Science Reports of the Tohoku Imperial University 1 Series vol. 14 (1925).

62) B. Baranowski and M. Smialowski: Phys. and Chem. Solids 12 (1960) 206.

63) R. J. Weiss: Proc. Phys. Soc. 82 (1963) 281.

64) J. Kanamori and Y. Teraoka: J. Magn. & Magn. Mater 10 (1979) 217.

65) H. Miwa: J. Magn. & Magn. Mater 10 (1979)223.

66) T. Moriya and K. Usami: Solid State Commun. 34 (1980) 95.

67) L. May: An Introduction to Mössbauer Spectroscopy (Plenum Press, New York, 1971).

68) H. Sano: Mössbauer Bunkoh-Gaku (Kodansha, Tokyo, 1972), in Japanese.

69) ed. U. Gonser: Topics in Applied Physics vol. 5 "Mössbauer Spectroscopy" (Springer-Verlag, New York, 1975).

70) B. Window: J. Phys. E4 (1971) 401.

71) F. E. Fujita: Topics in Applied Physics, vol. 5 "Mossbauer Spectroscopy", (Springer-Verlag, 1975), ed. V. Gonser.

72) S. Wakoh and J. Yamashita: J. Phys. Soc. Jpn. 21 (1966) 1712.

73) H. Hasegawa and J. Kanamori: J. Phys. Soc. Jpn. 31 (1971) 382.

74) S. Harada, S. Ohno and S. Tamaki: J. Phys. Soc. Jpn 44 (1978) 1787.

75) R. Ingalls: Phys. Rev. 155 (1967) 157.

76) ed. Kanbe Hirotaro: Netsubuseki (Kodansha, Tokyo, 1975), in Japanese.

77) ed. Nippon Kagaku Gakkai: Shin-Jikken-Kagaku Koza vol. 2 (Maruzen, Tokyo, 1977), in Japanese.

78) T. B. Flanagan and W. A. Oates: Ber. Bunsenges. Phys. Chem. 76 (1972) 706.

79) H. Frieske and E. Wicke: Ber. Bunsenges. Phys. Chem. 77 (1973) 50.

80) G. Alefeld: Ber. Bunsenges. Phys. Chem. 76 (1972) 746.

81) H. Wagner and H. Horner: Adv. Phys.23 (1974) 587.

82) H. Horner and H. Wagner: J. Phys. C7 (1974) 3305.

83) R. Mehlmann, H. Husemann and H. Brodowsky: Ber. Bunsenges. Phys. Chem. 77 (1973) 36.

84) H. A. Rafizadeh: Phys. Rev. 23 (1981) 1628.

85) H. Kanzaki: J. Phys. Chem. Solids. 2 (1957) 24.

86) C. Kittel: Introduction to Solid State Physics 4th ed. (Wiley,1971)

87) B. Baranowski, S. Majchrzak and T. B. Flanagan: J. Phys. F 1 (1971) 258.

88) A. C. Switendick: Ber. Bunsenges. Phys. Chem. 76 (1972) 535.

89) T. Tanabe, H. Adachi and S. Imoto: Japan J. Appl. Phys. 17 (1978) 49.